Mon. Not. R. Astron. Soc. **000**, 1–17 (2011) Printed 23 March 2012 (MN LATEX style file v2.2)

Rossiter-McLaughlin effect measurements for WASP-16, WASP-25 and WASP-31⋆

D. J. A. Brown[1]†, A. Collier Cameron[1], D. R. Anderson[2], B. Enoch[1], C. Hellier[2], P. F. L. Maxted[2], G. R. M. Miller[1], D. Pollacco[3], D. Queloz[4], E. Simpson[3], B. Smalley[2], A. H. M. J. Triaud[4], I. Boisse[5], F. Bouchy[5,6], M. Gillon[7], G. Hébrard[5,6]

[1] *SUPA, School of Physics and Astronomy, University of St Andrews, North Haugh, St Andrews, Fife KY16 9SS, UK.*
[2] *Astrophysics Group, School of Chemistry and Physics, Keele University, Staffordshire, ST5 5BG, UK.*
[3] *Astrophysics Research Centre, School of Mathematics & Physics, Queen's University, University Road, Belfast, BT7 1NN, UK.*
[4] *Observatoire Astronomique de l'Université de Genève, Chemin des Maillettes 51, CH-1290 Sauverny, Switzerland*
[5] *Institut d'Astrophysique de Paris, UMR7095 CNRS, Université Pierre & Marie Curie, 98bis Bd Arago 75014 Paris, France*
[6] *Observatoire de Haute Provence, CNRS/OAMP, 04870 St Michel l'Observatoire, France*
[7] *Institut d'Astrophysique et de Géophysique, Université de Liège, Allée du 6 Août 17, Bat. B5C, Liége 1, Belgium*

Accepted 2012 March 22

ABSTRACT

We present new measurements of the Rossiter-McLaughlin (RM) effect for three WASP planetary systems, WASP-16, WASP-25 and WASP-31, from a combined analysis of their complete sets of photometric and spectroscopic data. We find a low amplitude RM effect for WASP-16 (Teff $= 5700 \pm 150$ K), suggesting that the star is a slow rotator and thus of an advanced age, and obtain a projected alignment angle of $\lambda = -4.2^{\circ}{}^{+11.0}_{-13.9}$. For WASP-25 ($T$eff $= 5750 \pm 100$ K) we detect a projected spin-orbit angle of $\lambda = 14.6^{\circ} \pm 6.7$. WASP-31 ($T$eff $= 6300 \pm 100$ K) is found to be well-aligned, with a projected spin-orbit angle of $\lambda = 2.8^{\circ} \pm 3.1$. A circular orbit is consistent with the data for all three systems, in agreement with their respective discovery papers. We consider the results for these systems in the context of the ensemble of RM measurements made to date. We find that whilst WASP-16 fits the hypothesis of Winn et al. (2010) that 'cool' stars (Teff < 6250 K) are preferentially aligned, WASP-31 has little impact on the proposed trend. We bring the total distribution of the true spin-orbit alignment angle, ψ, up to date, noting that recent results have improved the agreement with the theory of Fabrycky & Tremaine (2007) at mid-range angles. We also suggest a new test for judging misalignment using the Bayesian Information Criterion, according to which WASP-25 b's orbit should be considered to be aligned.

Key words: planetary systems – stars:individual:WASP-16 – stars:individual:WASP-25 – stars:individual:WASP-31 – techniques:radial velocities

1 INTRODUCTION

As the number of transiting "hot Jupiters" known to astronomy has grown, there has been a gradually increasing push towards fully categorising their physical and orbital properties. It is widely presumed that close-in gas giants do not form at the locations in which we observe them, and there are competing theories to describe the process that leads them to their observable orbits.

Migration induced by a protoplanetary disc provides one means by which such a situation can be explained (Lin, Bodenheimer & Richardson 1996). Since such discs are generally aligned with the host star owing to angular momentum conservation, we would expect that disc migration would preferentially produce well-aligned hot Jupiter systems. Some misaligned planets would not be out of place under this mechanism, being the result of close planet-planet

⋆ based on observations made using the CORALIE high resolution échelle spectrograph mounted on the 1.2 m *Euler* Swiss Telescope and the HARPS high resolution échelle spectrograph mounted on the ESO 3.6 m (under proposals 084.C-0185 & 085.C-0393), both at the ESO La Silla observatory.

† E-mail:djab@st-andrews.ac.uk

encounters following migration, but we would expect the majority of planets to exhibit spin-orbit alignment.

The Kozai-Lidov mechanism (Kozai 1962; Lidov 1962) is the basis of a competing theory for which evidence is mounting. The presence of a third, outer body in a planetary system can excite periodic oscillations in both the eccentricity and inclination of a planetary orbit; inward migration then follows, with tidal friction kicking in as the planet approaches its host, causing the orbit to shrink and circularise (Fabrycky & Tremaine 2007). The oscillating inclination that results from Kozai-Lidov interactions produces a continuum of inclinations once the orbits are stable, and thus we would expect the majority of hot Jupiters to exhibit misaligned orbits if the Kozai-Lidov mechanism operates.

It is possible, to some extent, to distinguish between these competing theories through measurement of the spin-orbit alignment angles of hot Jupiter systems. Given the different angular distributions predicted by these theories, building up a significant number of spin-angle measurements is a useful means of determining which mechanism is acting. Unfortunately the true misalignment angle cannot be measured unless a spectroscopic measurement of $v \sin I$ is made, and the stellar rotation period is known. This yields an estimate of the inclination axis to the line-of-sight (e.g. Schlaufman (2010)). The situation is made more difficult by systematic uncertainties in $v \sin I$ measurements, and the sine function, which flattens as it approaches 90° and therefore only yields useful measurements at low to intermediate inclinations. We are thus currently limited to measuring he projected spin-orbit misalignment angle in the plane of the sky. This is generally measured through the Rossiter-McLaughlin (RM) effect (Rossiter 1924; McLaughlin 1924) which is observable during transit. As the planet transits the approaching limb of the star its spectrum is red-shifted, and when it transits the receding limb its spectrum is blue-shifted. The precise form of the RM anomaly in the radial velocity (RV) curve gives the projected misalignment angle, λ.

The first observation of the RM effect for a transiting planet was made by Queloz et al. (2000), and since then the number of measurements has increased significantly to a level such that it is possible to begin carrying out analysis of the ensemble of measurements. Fabrycky and Winn (2009) investigated 11 systems with known values of λ, deriving two theoretical distributions for ψ, the true misalignment angle, using different assumptions about the form of the distribution. They suggested, based on an apparent dual population within their data set, that there might be two routes for planet migration, one producing mostly aligned planets and the other producing misaligned planets.

One early indication of a pattern was that misaligned planets tended to be high mass and on eccentric orbits (Johnson et al. 2009). Subsequent observations have often countered this initial trend (for example HAT-P-7 (Winn et al. 2009; Narita et al. 2009)), but high mass ($M_P > 4\,M$Jup) planets do appear to have a different obliquity distribution (Hébrard et al. 2011). Of the 6 planets in this category with measured misalignment angles four are misaligned, but none have $|\lambda| > 50°$. More observations of high mass planets are needed before we can be certain that this is not merely an artefact of small-number statistics however.

One of the more intriguing suggestions was put forward by Winn et al. (2010) (hereafter W10), who speculated that the division into aligned and misaligned planets might be dependent on the effective temperature of the host star. Using a larger sample of 19 systems with known λ, they found that the misaligned systems were preferentially hotter than the aligned examples, with a critical temperature of Teff ≈ 6250 K dividing the two populations. One explanation put forward for this was the tidal realignment of planets around 'cool' stars, with the equivalent process around 'hot' stars being suppressed owing to their lack of a convective envelope. W10 further conjecture that the current ψ distribution could be completely explained by a migration mechanism driven by a combination of Kozai-Lidov oscillations and planet-planet scattering, without the need to invoke disc migration.

Triaud et al. (2010) (hereafter T10) added 6 planets to the ensemble of known RM measurements. Calculating individual ψ distributions for each planet based on the assumption that stellar rotation axes are randomly oriented on the sky, they produced a total distribution for the ensemble of planets, finding that it matched the theoretical distribution of Fabrycky & Tremaine (2007) for Kozai-Lidov mechanism dominated migration, further implying that disc migration might be superfluous to requirements for explaining the presence of hot Jupiters.

Here we present measurements of the RM angle for three more planets from the Wide Angle Search for transiting Planets (WASP) (Pollacco et al. 2006), WASP-16 b, WASP-25 b and WASP-31 b, and investigate how they modify the ensemble results and conclusions discussed above. In section 2 we give details of our observations, and in section 3 we discuss the analytical methods used to determine the misalignment angles. In section 4 we report on the results of our analysis for the individual systems. In section 5 we discuss the implications of our results for previously observed trends. Finally, in section 6, we take another look at the question of alignment, presenting a new test for planetary orbit misalignment.

2 OBSERVATIONS

Radial velocity data for all three planetary systems were obtained using the CORALIE high precision échelle spectrograph (Queloz et al. 2000b) mounted on the Swiss 1.2 m Euler telescope, and with the HARPS high precision échelle spectrograph (Mayor et al. 2003) mounted on the 3.6 m ESO telescope at La Silla. Data from CORALIE were used primarily to constrain the presence of a long-term trend in radial velocity that might be indicative of a third body in the system, whilst HARPS was used to monitor the radial velocity before, during and after a specific transit event. Two data points were obtained the night before the transit, and for at least one night following the transit; on the night of the transit observations were started 90 minutes prior to the predicted start of transit and continued until 90 minutes after its predicted conclusion.

2.1 WASP-16

WASP-16 was observed using CORALIE between 2008 March 10 and 2009 June 3, on an ad-hoc basis. One datum

Table 1. System parameters for the three WASP planetary systems for which we evaluate the Rossiter-McLaughlin effect. Parameters for WASP-16 were taken from Lister et al. (2009). Parameters for WASP-25 were taken from Enoch et al. (2011). Parameters for WASP-31 were taken from Anderson et al. (2011). $v \sin I$ and macroturbulence values have been updated through spectroscopic analysis of the new HARPS data using the Bruntt et al. (2010) calibration.

Parameter	Unit	WASP-16	WASP-25	WASP-31
M_*	$M_\odot$	$1.022^{+0.074}_{-0.129}$	1.00 ± 0.03	1.161 ± 0.026
R_*	$R_\odot$	$0.946^{+0.057}_{-0.052}$	0.92 ± 0.04	1.241 ± 0.039
Teff	K	5700 ± 150	5750 ± 100	6300 ± 100
$v \sin I$	$\mathrm{km\,s^{-1}}$	2.3 ± 0.4	2.6 ± 0.4	8.1 ± 0.5
macroturbulence	$\mathrm{km\,s^{-1}}$	2.3	2.4	4.2
M_p	MJup	$0.855^{+0.043}_{-0.076}$	0.58 ± 0.04	0.478 ± 0.030
R_p	RJup	$1.008^{+0.083}_{-0.060}$	$1.22^{+0.06}_{-0.05}$	1.537 ± 0.060
P	days	3.11860 ± 0.00001	3.764825 ± 0.000005	3.405909 ± 0.000005
a	AU	$0.0421^{+0.0010}_{-0.0019}$	0.0473 ± 0.0004	0.04657 ± 0.00034
e		0(adopted)	0(adopted)	0(adopted)
i	$^\circ$	$85.22^{+0.27}_{-0.43}$	88.0 ± 0.5	84.54 ± 0.27

was also acquired on 2010 July 14 to retest the hypothesis of a long-term radial velocity trend. The transit observed with HARPS occurred on the night of 2010 March 21; 32 data points were acquired over the duration of the night. This transit observation was affected by cloud cover, so an additional transit was observed on the night of 2011 May 12, producing a further 28 RV measurements. Further measurements were made on the days surrounding this transit as well (see journal of observations, Tables B1, B2 and B3).

Details of the photometric observations of WASP-16 are given in Lister et al. (2009).

2.2 WASP-25

HARPS observed the transit taking place on the night of 2008 April 11. 44 observations were made that night, with additional data acquired on adjacent nights (see the journal of observations, Tables B4 and B5). The system was observed using CORALIE between 2008 December 29 and 2009 June 28, with observations made at irregular intervals between these dates.

Enoch et al. (2011) describe the photometric observations that were made of WASP-25.

2.3 WASP-31

WASP-31 was observed using CORALIE between 2009 January 4 and 2010 May 18 during several short runs. HARPS was used to observe a full transit on the night of 2010 April 15, with 17 data points obtained. Additional observations were made on adjacent nights (see the journal of observations, Tables B6 and B7).

The photometric observations for WASP-31 are discussed in Anderson et al. (2011).

3 DATA ANALYSIS

Our analysis mirrors that of T10, using the complete set of photometric and spectroscopic data for the objects that we investigate in order to fully account for parameter correlations. We use an adapted version of the code described in Collier Cameron et al. (2007), fitting models of the photometric transit, the Keplerian RV and the RM effect to the system data. The fit of our model is refined using a Markov Chain Monte Carlo (MCMC) technique to minimize the χ^2 statistic, and to explore the parameter space using the jump parameters T_0 (epoch of mid-transit), P (orbital period), W (transit width), b (impact parameter), γ velocity, $\dot{\gamma}$, K (RV semi-amplitude), Teff (stellar effective temperature), $[Fe/H]$ (metallicity), $\sqrt{e}\cos\omega$, $\sqrt{e}\sin\omega$, $\sqrt{v \sin I}\cos\lambda$ and $\sqrt{v \sin I}\sin\lambda$. We use a burn-in phase of 2000 steps, with burn-in judged to be complete when χ^2 becomes greater than the median of all previous values (Knutson et al. 2008). A minimum burn-in length of 500 steps is applied to ensure that burn-in is truly complete. Once this initial phase is over we use a further 100 steps to recalculate the parameter jump lengths before beginning the real Markov Chain of 10000 accepted steps; with the acceptance rate of 25 percent recommended for the Metropolis-Hastings algorithm (Tegmark et al. 2004) this gives an effective chain length of 40000 steps. Our set of final parameters is taken to be the median of the Markov chain, with the 1σ error bars calculated from the values that encompass the central 68.3 percent of the accepted steps. We account for limb darkening using a non-linear treatment based on the tables of Claret (2000), interpolating the coefficients at each step in the chain.

The inclusion of the photometric data is an important point. Although we fit the RM effect to the radial velocity data, the transit width and depth, as well as the impact parameter, can be determined from the photometric transit. These parameters have a role to play in the characterisation of the form of the RM anomaly. The transit width helps to determine the duration of the anomaly whilst the depth gives the planetary and stellar radii. The radii and impact

parameter in turn help to determine $v \sin I$, upon which the amplitude of the anomaly depends (Queloz et al. 2000). Although characterisation of the RM effect can be carried out using the spectroscopic data alone, by taking the photometric data into account in this way we ensure consistency across the full set of system parameters. To account for stellar jitter we initially assign a value of $1\,\mathrm{m\,s^{-1}}$, below the level of precision of the spectrographs used for this work, which we added in quadrature to the in-transit photometric data.

We separate our RV data by instrument, and within those distinctions also treat spectroscopic data taken on nights featuring planetary transits as separate datasets. Our model for the orbital RV signature treats the sets of data as independent, producing individual offsets and radial velocity trends for each one. The reported solution is that for the set of RV data covering the greatest phase range. For completeness, we also repeated our analysis using *only* RV data taken during nights that featured a transit event, but found little to distinguish them from our analysis of the the full set of data.

For our RM model we use the analytic formula of Hirano et al. (2011). This method requires prior knowledge of several broadening coefficients, specifically the macroturbulence, for which our estimates are noted in Table 1, and the Lorentzian (γ) and Gaussian (β) spectral line dispersions. The line dispersions were dictated by our use of the HARPS instrument, which has a spectral resolution of $R = 115000$, implying an instrumental Gaussian dispersion of $2.61\,\mathrm{km\,s^{-1}}$. This was combined with the intrinsic Doppler linewidth, including appropriate thermal and turbulent motion for each star, to obtain values of $\beta = 3.1\,\mathrm{km\,s^{-1}}$ for WASP-16 and WASP-25, and $\beta = 3.3\,\mathrm{km\,s^{-1}}$ for WASP-31. We assumed $\gamma = 0.9\,\mathrm{km\,s^{-1}}$ in line with Hirano et al., and also assumed that the coefficient of differential rotation, $\alpha = 0$. WASP-16 and WASP-25 are both slow rotators, and whilst WASP-31 should be considered a moderately fast rotator, without knowledge of the inclination of the stellar rotation axis it is difficult to place a value of α.

We apply several Bayesian priors to χ^2 to account for previously known information: a prior on the eccentricity, allowing for the forcing of circular solutions; a prior on the spectroscopic $v \sin I$, using updated values of $v \sin I$ derived from the newly acquired HARPS spectra and the macroturbulence calibration of Bruntt et al. (2010), and a prior enforcing a main sequence (MS) mass-radius relationship. This MS prior is based on that discussed in Collier Cameron et al. (2007), but is only applied to the stellar radius. The stellar mass is estimated using the calibration of Enoch et al. (2010).

To distinguish between models that use different combinations of priors we minimize the reduced χ^2 for the spectroscopic data; in cases where there is little to choose between the different sets of input conditions we gravitate towards the model with the fewest free parameters. In what follows we refer to χ^2 as the combined χ^2 for the complete data set, χ^2_{RV} as the value for the spectroscopic RV data only, and χ^2_{red} as the reduced χ^2 for the spectroscopic data alone. Note also that we refer to the projected spin-orbit misalignment angle as λ, as is more common in the literature, not β as used by T10 (strictly $\lambda = -\beta$).

4 ROSSITER-MCLAUGHLIN RESULTS

4.1 WASP-16

WASP-16b (Lister et al. 2009) (hereafter L09) is a close Jupiter analog orbiting a Solar-type star with a period of 3.12 days. The planet is somewhat less massive than Jupiter but of comparable radius, whilst the host star is similar in mass, radius and metallicity to the Sun, but exhibits significant lithium depletion. Our updated spectroscopic analysis using the HARPS spectra yields a projected stellar rotation velocity of $v \sin I = 2.3 \pm 0.4\,\mathrm{km\,s^{-1}}$.

Our original estimate of stellar jitter produced fits with $\chi^2 \approx 1.6$, leading us to re-estimate the jitter following Wright (2005). We calculated line strengths for the calcium H and K emission lines in each of the HARPS spectra, and used these to estimate values for the chromospheric activity metric S. These were then calibrated against the Mount Wilson sample (see e.g. Baliunas et al. (1995)), and absolute magnitudes of the stars were calculated using Gray (1992). We eventually adopted the 20th percentile value of $3.6\,\mathrm{m\,s^{-1}}$ as a conservative estimate of the jitter.

Removing the requirement for the system to obey a main sequence mass-radius relationship (equation 6 in Collier Cameron et al. (2007)) produced changes of between 0 and 2 percent in the stellar mass and radius, leading to increases in the stellar density of between 1 and 4 percent, for no discernible improvement in fit. Comparing impact parameter values, we find that we obtain an average value of $\bar{b} = 0.83^{+0.03}_{-0.04}$ for the cases both with and without the MS prior active. The parameter S (Collier Cameron et al. 2007),

$$S = -2 \ln P(M_*, R_*) = \frac{R_* - R_0}{\sigma_R^2}, \quad (1)$$

used to measure the discrepancy between the stellar radius from the (J-H) colour and that returned by the MCMC algorithm, increases from an average of 0.17 to 0.34 when the prior is removed, a relatively small increase as suggested by the modest changes in stellar parameters. We therefore find little to distinguish between the cases with the MS requirement applied, and those with the stellar radius freely varying, and choose not to apply this prior in our final solution.

Adding a long-term, linear RV trend produced no improvement in χ^2_{red}, and with a magnitude of $|\dot{\gamma}| < 3\,\mathrm{m\,s^{-1}\,yr^{-1}}$ we disregard the possibility that there is a such a trend in the spectroscopic data. Adding a prior on the spectroscopic $v \sin I$ similarly gave almost no difference in the quality of the fit obtained. For most combinations of priors our analysis returned $v \sin I \approx 1.2 \pm 0.3\,\mathrm{km\,s^{-1}}$, significantly slower than the spectroscopic value.

Allowing the eccentricity to float again led to no significant improvement in the fit, and all of the values of e returned by our various combinations of priors were consistent with $e = 0$ to within 2σ. We tested these small eccentricity values using equation 27 of Lucy & Sweeney (1971), which adopts a null hypothesis of a circular orbit and considers an orbit to be eccentric if this is rejected at the 5 percent significance level. This F-test indicated that none of the eccentricities were significant, and thus that a circular orbit is favoured.

We therefore adopt as our conclusive solution the case without the MS prior active, with no prior on $v \sin I$, no

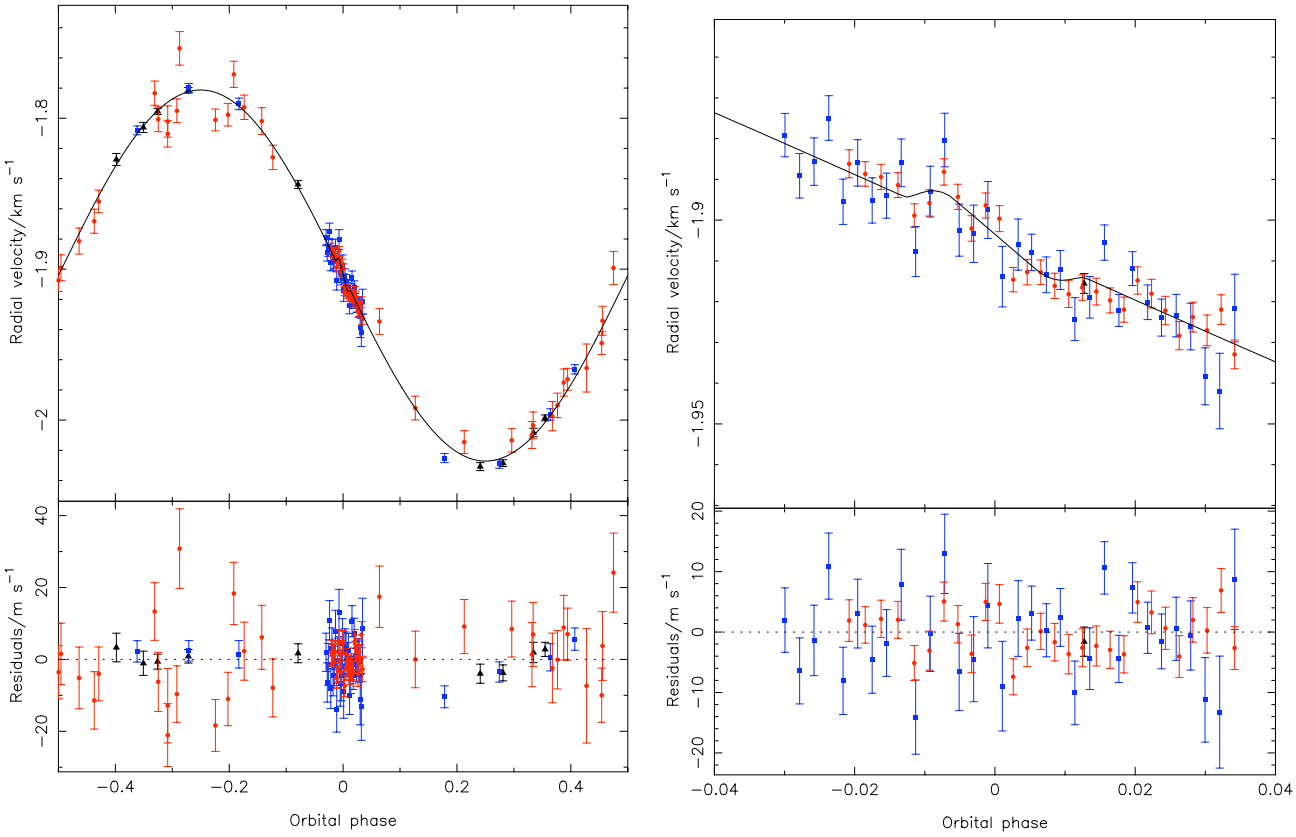

Figure 1. Results from the fit to the data for WASP-16 using $e = 0$, no long-term radial velocity trend, no prior on the spectroscopic $v \sin I$, and without forcing the mass-radius relationship. Black, filled triangles represent data from CORALIE. Blue, filled squares represent data from the first HARPS run. Red, filled circles represent data from the second HARPS run. The best-fitting model is plotted as a solid black line. *Top left:* Complete radial velocity reflex motion curve. *Bottom left:* Residuals from theRV fit, exhibiting no correlation with phase. *Top right:* Close up of the transit region from the radial velocity curve showing the RM effect, along with the residuals. *Bottom right:* Residuals for the RV data within the RM window.

long-term trend in velocity and a circular orbit, but we stress that changing the priors had little impact on the parameter values returned by the MCMC algorithm. Our adopted solution returns values of $\lambda = -4.2^{\circ}{}^{+11.0}_{13.9}$ and $v \sin I = 1.2^{+0.4}_{-0.5}\,\mathrm{km\,s^{-1}}$; this is significantly slower than the spectroscopic value of $v \sin I$ that we obtained from spectral analysis. However an alternative analysis of the HARPS spectra using the calibration of Gray (2008) provides an estimate of $v \sin I = 1.2 \pm 0.5$, in good agreement with the value that we found from our model. Our solution also indicates a high impact parameter of $0.82^{+0.01}_{-0.02}$ that reduces the likelihood of a degeneracy developing between λ and $v \sin I$. Examination of Fig. 2b highlights this, with a triangular distribution that is centred close to $\lambda = 0^{\circ}$. The main section of this distribution lies within the limits $|\lambda| < 20^{\circ}$, providing further evidence for the well-aligned system that was suggested by our best-fitting RM angle. From L09 we note that the host star has $T\mathrm{eff} = 5700 \pm 150\,\mathrm{K}$, which places it in the 'cool' category of W10; an aligned orbit therefore fits their hypothesis quite nicely.

As previously noted, the amplitude of the RM anomaly for WASP-16 is quite small. The aligned nature of the system suggests that this can be put down to the star being an old, slowly rotating star, which would be consistent with the age estimate reported by L09, which suggests an age $> 5\,\mathrm{Gyr}$ based on a lack of detectable lithium. A second possible explanation could be that we are in fact viewing the host star almost pole-on, which could still be consistent with an orbit that is aligned in the plane of the sky. This would lead to a low projected rotation velocity, and a transit across the pole of the star would have a small RM amplitude, as observed here. The minimum stellar inclination is limited by the observed lithium depletion[1], but such a structure would imply a younger age for the star owing to the rapid true stellar rotation. Interestingly isochronal analysis in L09 implies an age of $2.3^{+5.8}_{-2.2}$ Gyr, lower than the limit implied by the lithium depletion. However new isochronal fits, using our results and a range of stellar models, returned ages of $4.7^{+3.3}_{-4.3}$ Gyr (Padova models; Marigo et al. (2008)), $4.8^{+1.2}_{-3.3}$ Gyr (Yonsei-Yale models; Demarque et al. (2004)), $6.0^{+5.0}_{-4.0}$ Gyr (Teramo models; Pietrinferni et al. (2004)) and $5.0^{+4.9}_{-3.8}$ Gyr (VRSS models; VandenBerg, Berg-

[1] The abundance of lithium gives us a minimum age, as stated. If we assume that gyrochronology is applicable, then this provides a maximum true stellar rotation velocity. This in turn allows us to use the detected $v \sin I$ to calculate the minimum possible stellar inclination.

Table 2. A comparison of the χ^2 and χ^2_{red} values for WASP-16 for each combination of Bayesian priors. All values of χ^2 include the Bayesian penalties applicable for that combination of priors.

$v \sin I$ prior	MS prior	$\dot{\gamma}$/ms^{-1}yr^{-1}	eccentricity	$v \sin I$/km s^{-1}	λ/°	χ^2	χ^2_{RV}	χ^2_{red}
off	off	0	$0.009^{+0.010}_{-0.006}$	1.2 ± 0.4	$-2.1^{+10.5}_{-11.0}$	12915 ± 161	100 ± 14	0.9 ± 0.1
off	on	0	$0.004^{+0.006}_{-0.002}$	$1.2^{+0.4}_{-0.5}$	$-2.8^{+10.7}_{-11.1}$	12917 ± 161	102 ± 14	0.9 ± 0.1
off	off	$1.0^{+0.8}_{-0.8}$	$0.011^{+0.009}_{-0.007}$	$1.0^{+0.5}_{-0.6}$	$-2.5^{+13.6}_{-16.6}$	12912 ± 161	99 ± 14	0.9 ± 0.1
off	on	$0.6^{+0.5}_{-0.3}$	$0.007^{+0.007}_{-0.005}$	$1.1^{+0.4}_{-0.6}$	$-3.6^{+10.9}_{-14.8}$	12911 ± 161	99 ± 14	0.9 ± 0.1
off	off	0	0	$1.1^{+0.5}_{-0.6}$	$-6.7^{+11.7}_{-19.2}$	12917 ± 161	103 ± 14	1.0 ± 0.1
off	on	0	0	$1.2^{+0.4}_{-0.5}$	$-4.2^{+11.0}_{-13.9}$	12916 ± 161	103 ± 14	1.0 ± 0.1
off	off	0.1 ± 0.1	0	$1.1^{+0.5}_{-0.6}$	$-5.8^{+10.6}_{-14.5}$	12917 ± 161	102 ± 14	0.9 ± 0.1
off	on	$0.9^{+1.0}_{-0.9}$	0	1.2 ± 0.5	$-6.0^{+10.3}_{-15.4}$	12911 ± 161	102 ± 14	0.9 ± 0.1
2.3 ± 0.4	off	0	$0.011^{+0.009}_{-0.008}$	1.2 ± 0.3	$-1.8^{+11.0}_{-11.2}$	12910 ± 161	100 ± 14	0.9 ± 0.1
2.3 ± 0.4	on	0	$0.012^{+0.009}_{-0.007}$	1.2 ± 0.2	$-2.3^{+10.5}_{-11.7}$	12914 ± 161	98 ± 14	0.9 ± 0.1
2.3 ± 0.4	off	0.1 ± 0.1	$0.010^{+0.009}_{-0.007}$	1.2 ± 0.3	$-3.6^{+11.7}_{-11.3}$	12916 ± 161	101 ± 14	0.9 ± 0.1
2.3 ± 0.4	on	$0.7^{+0.7}_{-0.8}$	$0.011^{+0.009}_{-0.007}$	1.2 ± 0.2	$-2.9^{+9.9}_{-9.0}$	12912 ± 161	99 ± 14	0.9 ± 0.1
2.3 ± 0.4	off	0	0	1.2 ± 0.3	$-4.9^{+10.0}_{-11.0}$	12912 ± 161	102 ± 14	0.9 ± 0.1
2.3 ± 0.4	on	0	0	1.2 ± 0.3	$-4.8^{+9.6}_{-10.2}$	12919 ± 161	104 ± 14	1.0 ± 0.1
2.3 ± 0.4	off	$2.1^{+3.3}_{-1.8}$	0	$1.1^{+0.3}_{-0.4}$	$-5.6^{+10.0}_{-12.9}$	12916 ± 161	101 ± 14	0.9 ± 0.1
2.3 ± 0.4	on	$-0.6^{+1.6}_{-1.3}$	0	1.1 ± 0.4	$-5.7^{+11.4}_{-12.5}$	12917 ± 161	103 ± 14	0.9 ± 0.1

busch & Dowler (2006)). These ages further support the case for a slowly rotating host star, and are consistent with the star's observed lithium abundance.

Careful analysis of the HARPS spectra allowed us to measure the chromospheric Ca II H & K emission. We find that $\log(R'_{HK}) = -5.10 \pm 0.15$, indicating a low level of chromospheric activity. This rules out the possibility that the star is misaligned along the line-of-sight, as we would expect much greater calcium emission from a young, rapidly rotating star. We note that this agrees with the work of Schlaufman (2010), who finds no evidence for line-of-sight misalignment in the WASP-16 system. Following Watson et al. (2010) we calculate $P_{rot} = 30.2^{+4.7}_{-3.8}$ days, which implies an age of $3.8^{+1.2}_{-0.8}$ Gyr for WASP-16 according to the gyrochronology method of Barnes (2007) using the updated coefficients of Meibom, Mathieu & Stassun (2009) and James et al. (2010). A recent reanalysis of the WASP-1 and WASP-2 systems (Albrecht et al. 2011) highlighted the fact that in systems with low amplitude, low S/N RM anomalies, the angles reported tend towards 0° and 180° owing to the greater probability density in the distribution for λ. The same study cautions readers against drawing strong conclusions of alignment in such cases. Our data for WASP-16 certainly show some of the characteristics discussed in the Albrecht et al. study, and we have indeed found a well-aligned system with λ close to 0.

However there are other methods by which the alignment angle of a planetary orbit can be deduced. Doppler tomography is an established method for mapping velocity variations in binary stars (e.g. Albrecht et al. (2007, 2009)), but its application to transiting exoplanets is in its infancy. The technique has, to date, been used to study HD189733 (Collier Cameron et al. 2010), WASP-33 (Collier Cameron et al. 2010) and WASP-3 (Miller et al. 2010), and is best suited to analysing hot, rapidly rotating exoplanet host stars. WASP-16 A exhibits neither of these attributes, but analysis is ongoing (Miller et al., *in prep*) and indications are that it gives similar results for the obliquity angle of this system. An independent detection of the RM effect, also suggesting alignment, was announced at IAU Symposium 276 by Winn, and we look forward to the published results with interest.

4.2 WASP-25

WASP-25b (Enoch et al. 2011) (hereafter E11) is a significantly bloated, sub-Jupiter mass planet orbiting a solar-type, somewhat metal-poor host star with an orbital period of 3.76 days. A full set of results from our analysis is displayed in Table 3. One RV measurement was found to lie at $3\,\sigma$ from the best-fitting model, and to be consistent with the out of transit RV curve. This datum was omitted from our analysis, and will be discussed further later.

We found that allowing the eccentricity to float led to a negligible difference in χ^2_{red}, and that the eccentricity values being found were within 2σ of 0. We therefore concluded that the small eccentricity values being returned were arising owing to the biases inherent in the MCMC method (Ford 2006), and that the orbit of WASP-25 is circular. In this we agree with E11. We confirmed this conclusion regarding a circular orbit using the F-test of Lucy & Sweeney (1971), which returned very high probabilities of the small eccentricity values having arisen by chance.

We found little difference between the quality of fit for the equivalent cases with the MS mass-radius relation forced on the system, and those without the same constraint. The relaxation of this prior leads to larger values of λ, but also increases the discrepancy between the stellar mass and radius

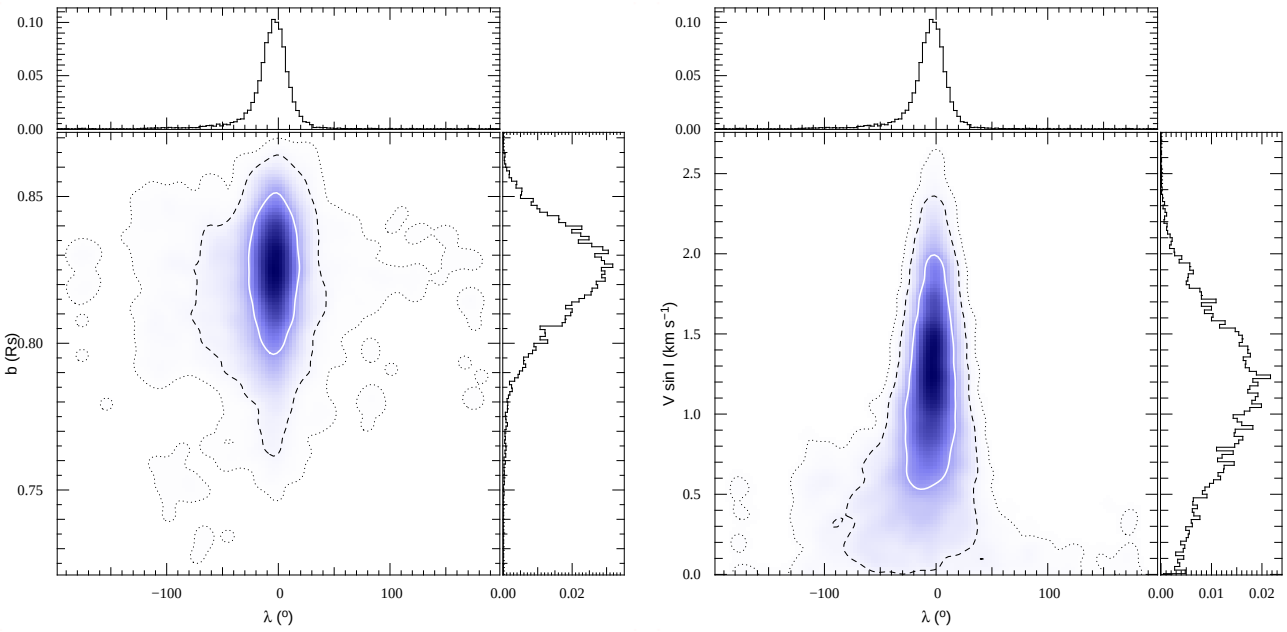

Figure 2. Posterior probability distributions derived from the Markov chains, for the fit to WASP-16 described in Fig. 1. The white contours mark the 62.87 percent confidence regions, the black, dashed contours the 95.45 percent confidence regions, and the black, dotted contours the 99.73 percent confidence regions. Marginalised, 1D distributions are displayed in the side panels. *Left:* b and λ. *Right:* $v \sin I$ and λ. This distribution has a triangular shape, and $\lambda = 0$ falls within the central body of the distribution. Both distributions have poorly constrained 99.73 percent confidence regions, and show a slight bias towards negative values of λ.

values. The stellar mass value varies little between runs, but relaxing the MS prior reduces the stellar radius by between 2 and 3 percent, dependent on the other priors being applied. This leads to an increase in the stellar density of between 7 and 12 percent from $\bar{\rho}_{*,\,MS} \approx 1.22\rho_{\odot}$ to $\bar{\rho}_{*,\,no\,MS} \approx 1.34\rho_{\odot}$, averaged across all combinations of the other priors. Considering the impact parameter, we find that relaxing the MS requirement gives a value of $\bar{b} = 0.38^{+0.16}_{-0.22}$, whilst using the prior returns $\bar{b} = 0.44^{+0.11}_{-0.12}$, both averaged across all other combinations of priors. The S parameter increases from an average of 3.56 to 5.92 when the prior is removed. In light of these differences, we elect to apply the MS prior in our final analysis.

Adding a long-term linear trend in RV improved the χ^2_{spec} of the solution, but the value of the trend varied significantly between runs, ranging from ≈ 2 to $\approx 105\,\mathrm{m\,s^{-1}\,yr^{-1}}$. We also found that in some cases the models produced when a trend was applied showed a notable offset from the RV data in transit. To check whether a trend was truly present in the system, 2 additional RV measurements were obtained using HARPS on 2010 August 25 and 26. Analysing these in conjunction with previously obtained data shows no evidence for a long-term RV trend, and so we disregard this possibility for our final solution. Introducing a prior on the spectroscopic $v \sin I$ produced no improvement to the quality of fit to the data, irrespective of the other flags. We do not therefore apply such a prior in our final solution, and take this opportunity to obtain a separate measurement of the projected stellar rotation speed.

Taking the results of these investigations into account, we select the solution with $e = 0$, no long-term linear trend in RV and no prior on $v \sin I$, with the main sequence mass-radius relation enforced. This gives $\lambda = 14.6^{\circ} \pm 6.7$, a detection of the RM effect at 2.2σ from 0. We also obtain a value for the stellar rotation of $v \sin I = 2.9 \pm 0.3\,\mathrm{km\,s^{-1}}$, slightly greater than but in agreement with our updated spectroscopic value of $2.6 \pm 0.4\,\mathrm{km\,s^{-1}}$. The impact parameter for this solution is 0.44 ± 0.04. No correlation is apparent between $v \sin I$ and λ (see figure 4b), although there is evidence for a correlation between the impact parameter and λ (see figure 4a). It is possible that this correlation is responsible for the poor fit of the model to some parts of the RM data.

The mechanism responsible for the outlier that we omitted from our analysis is unknown, although we note that Simpson et al. (2010) experienced a similar situation in their analysis of the WASP-38 system, positing seeing changes of telescope guiding faults as possible causes. We suggest a third mechanism; the discrepant point might be caused by the planet traversing a stellar spot. In such a situation the spot would mask the presence of the planet, causing the RV measurement to diverge from the standard RM anomaly pattern. This scenario was suggested to explain a similar anomaly in the data for the WASP-3 system (Tripathi et al. 2010), but we note that the divergence from the RM effect in that case showed a gradual rise and fall rather than the delta function change observed here, and was eventually attributed to the effect of moonlight. Unfortunately we lack simultaneous photometry from the night of the observed spectroscopic transit, which would show the presence of such a spot. It is also possible that some form of transient event, such as a white light stellar flare, is responsible for the drastic, sudden change in measured RV for this point, although. Such events were discussed in the context of LQ Hya (Montes et al. 1999), and were observed to produce

Table 3. A comparison of the χ^2 and χ^2_{red} values for WASP-25 for each combination of Bayesian priors. All values of χ^2 include the Bayesian penalties applicable for that combination of priors.

$v \sin I$ prior	MS prior	$\dot{\gamma}$/ms^{-1}yr^{-1}	eccentricity	$v \sin I$/km s^{-1}	λ/°	χ^2	χ^2_{RV}	χ^2_{red}
off	off	0	$0.011^{+0.010}_{-0.008}$	2.8 ± 0.3	$17.9^{+9.8}_{-8.6}$	14200 ± 169	104 ± 14	1.3 ± 0.2
off	on	0	$0.013^{+0.013}_{-0.009}$	2.8 ± 0.3	$15.9^{+7.5}_{-7.3}$	14195 ± 168	103 ± 14	1.3 ± 0.2
off	off	$103.8^{+25.5}_{-29.6}$	$0.013^{+0.014}_{-0.009}$	2.9 ± 0.3	$16.8^{+9.5}_{-9.4}$	14184 ± 168	90 ± 13	1.1 ± 0.2
off	on	$-10.3^{+13.6}_{-10.1}$	$0.011^{+0.013}_{-0.008}$	2.8 ± 0.3	$14.9^{+6.6}_{-7.1}$	14197 ± 169	101 ± 14	1.3 ± 0.2
off	off	0	0	2.9 ± 0.3	14.6 ± 6.7	14200 ± 169	104 ± 14	1.3 ± 0.2
off	on	0	0	2.9 ± 0.3	$17.0^{+8.5}_{-8.1}$	14199 ± 169	103 ± 14	1.3 ± 0.2
off	off	$96.1^{+28.7}_{-26.6}$	0	2.8 ± 0.3	$18.8^{+10.1}_{-8.6}$	14189 ± 168	91 ± 13	1.1 ± 0.2
off	on	$2.4^{+0.4}_{-0.3}$	0	2.8 ± 0.2	$12.7^{+8.4}_{-5.7}$	13754 ± 166	103 ± 14	1.3 ± 0.2
2.6 ± 0.4	off	0	$0.013^{+0.014}_{-0.009}$	2.8 ± 0.2	$15.6^{+8.9}_{-8.4}$	14194 ± 168	103 ± 14	1.3 ± 0.2
2.6 ± 0.4	on	0	$0.011^{+0.011}_{-0.008}$	2.8 ± 0.2	$14.5^{+7.6}_{-6.7}$	14200 ± 169	104 ± 14	1.3 ± 0.2
2.6 ± 0.4	off	$100.4^{+28.6}_{-28.4}$	$0.013^{+0.014}_{-0.009}$	2.8 ± 0.2	$16.8^{+9.2}_{-9.0}$	14183 ± 168	90 ± 13	1.1 ± 0.2
2.6 ± 0.4	on	$97.1^{+28.0}_{-25.8}$	$0.011^{+0.013}_{-0.008}$	2.8 ± 0.2	$15.3^{+7.5}_{-6.6}$	14187 ± 168	91 ± 14	1.1 ± 0.2
2.6 ± 0.4	off	0	0	2.8 ± 0.2	$16.8^{+9.7}_{-8.8}$	14198 ± 169	104 ± 14	1.3 ± 0.2
2.6 ± 0.4	on	0	0	2.8 ± 0.2	$14.8^{+6.6}_{-6.9}$	14202 ± 169	104 ± 14	1.3 ± 0.2
2.6 ± 0.4	off	$104.8^{+21.9}_{-35.6}$	0	2.8 ± 0.2	$17.1^{+9.1}_{-7.9}$	14185 ± 168	91 ± 13	1.1 ± 0.2
2.6 ± 0.4	on	95.4 ± 26.5	0	2.8 ± 0.2	$14.5^{+6.7}_{-7.2}$	14189 ± 168	91 ± 13	1.1 ± 0.2

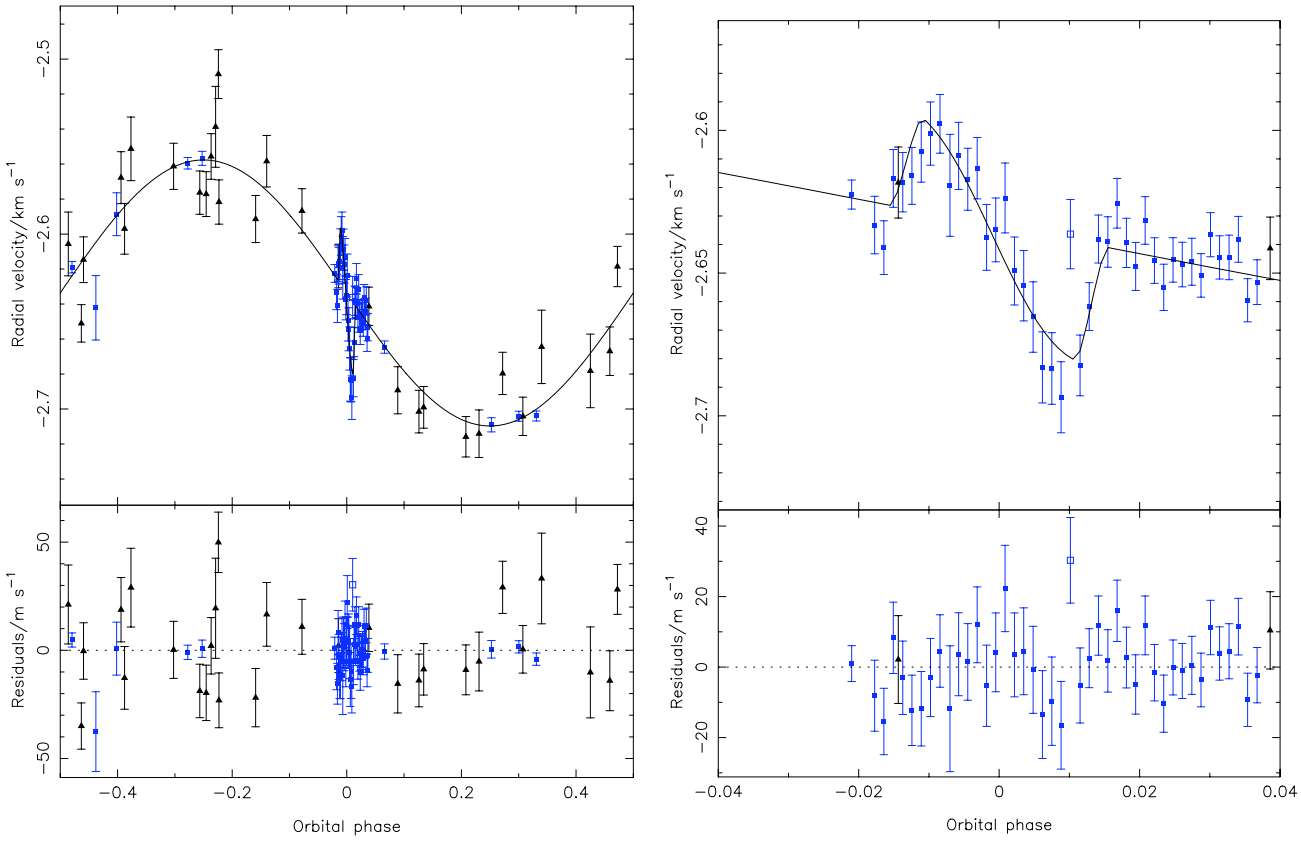

Figure 3. Results from the fit to the data for WASP-25 of our optimal solution: a circular orbit, no long-term RV trend and no prior on the spectroscopic $v \sin I$. The main sequence mass-radius relation was not enforced. The point denoted by the open square was found to lie $3\,\sigma$ from the best-fitting model, and was not included in the analysis. Legend as for Fig. 1.

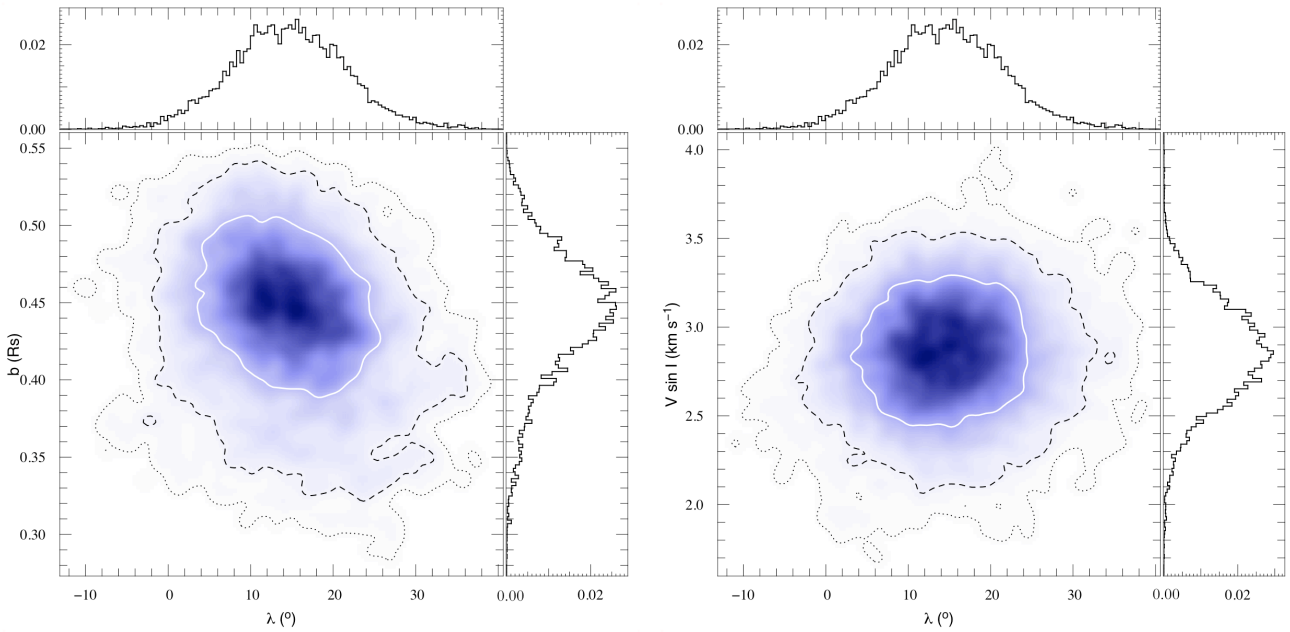

Figure 4. Posterior probability distributions, derived from the Markov chain, for the fit to the data for WASP-25 described in Fig. 3. Key as for Fig. 2. *Left:* b and λ. There are appears to be some small level of correlation between the two parameters. *Right:* $v \sin I$ and λ. $\lambda = 0$ falls outwith the 68.27 percent confidence contour, but within the 95.45 percent confidence contour, indicating a moderately significant detection of λ.

chromospheric disturbance in the core of otherwise normal spectral lines. This dilution of the spectral lines could affect the continuum level during the flare event, and potentially lead to anomalous redshifting for a short period of time. Such an event would have to be very short duration however, and coincide with the planet's path across the stellar disc.

Should we consider WASP-25 to be aligned? W10 put forward a criterion of $\lambda \geqslant 10^o$ to $> 3\sigma$ for misalignment; our result for WASP-25 clearly fails this test. T10 suggest an alternative criterion of $\lambda > 30^o$ as the limit above which we can be sure a system is misaligned given the average magnitude of the errors in λ that are found by analysis of the RM effect. WASP-25 also misses this target by some margin. But the data for the RM effect appear to be slightly asymmetric in Fig. 3b, suggesting that the system is misaligned (although we note that the best fitting model does not reflect this).

This slight asymmetry in the RM anomaly might arise as a result of some form of systematic effect. We have already mentioned the possibility of stellar spots in the context of the anomalous datum omitted from our analysis. Could they also provide a possible explanation for the asymmetry? Consider a star on which stellar spots are more numerous in one hemisphere than the other during the planetary transit, but on which they lie away from the transit chord. As the planet transits the more spotty hemisphere it will hide a comparatively larger fraction of the photosphere, and therefore mask a greater contribution to the overall flux than when it is transiting the less spotty hemisphere. The half of the anomaly corresponding to the spotted hemisphere would therefore have a greater amplitude than the half of the anomaly corresponding to the unspotted hemisphere, leading to an asymmetric RM effect. If the difference in the number and/or size of spots between the two hemispheres is small then the asymmetry would be only minor. This interesting systematic was discussed by Albrecht et al. (2011) for the case of WASP-2, and also seems to have played a role in the analysis of the CoRoT-2 RM in Bouchy et al. (2008). In the case of WASP-25 the approaching, blue-shifted hemisphere would be required to have a slightly greater density of stellar spots than the receding, red-shifted hemisphere, which would also lead back to the possibility of a transient event being responsible for the anomalous datum.

We will return to the question of WASP-25's alignment in section 6.

4.3 WASP-31

WASP-31 (Anderson et al. 2011) is a bloated, 0.5 M_J planet orbiting an F-type star of sub-solar metallicity with a period of 3.5 days. The host star is a moderately rapid rotator, with $v \sin I = 8.1 \pm 0.5$ from spectroscopy. Full results of our analysis can be found in Table 4.

We found no difference between the χ^2_{red} values for any combination of priors. We found that imposing the main-sequence mass-radius relation had little effect on the fit to the spectroscopic data, but had a deleterious effect on the stellar parameters. Removing the prior produced an increase in stellar radius of between 3 and 6 percent and a decrease in the stellar mass of between 1 and 2 percent, leading to a decrease in stellar density of between 8 and 15 percent from $\bar{\rho}_{*,\,MS} \approx 0.67\rho_\odot$ to $\bar{\rho}_{*,\,no\,MS} \approx 0.62\rho_\odot$, averaged across all other combinations of priors. Comparing the impact parameter and S statistic, we find $\bar{b} = 0.79^{+0.03}_{-0.05}$ and $\bar{S} = 10.2$ with no MS prior applied, and $\bar{b} = 0.77^{+0.03}_{-0.04}$ with $\bar{S} = 2.9$

Table 4. A comparison of the χ^2 and χ^2_{red} values for WASP-31 for each combination of Bayesian priors. All values of χ^2 include the Bayesian penalties applicable for that combination of priors.

$v \sin I$ prior	MS prior	$\dot{\gamma}/\mathrm{ms}^{-1}\mathrm{yr}^{-1}$	eccentricity	$v \sin I/\mathrm{km\,s}^{-1}$	$\lambda/^\circ$	χ^2	χ^2_{RV}	χ^2_{red}
off	off	0	$0.027^{+0.032}_{-0.019}$	7.5 ± 0.8	$2.8^{+1.1}_{-2.9}$	14703 ± 171	64 ± 11	0.9 ± 0.2
off	on	0	$0.031^{+0.029}_{-0.019}$	$7.7^{+0.9}_{-0.8}$	$3.6^{+2.9}_{-3.5}$	14708 ± 172	64 ± 11	0.9 ± 0.2
off	off	$6.1^{+8.1}_{-8.4}$	$0.023^{+0.031}_{-0.017}$	7.4 ± 0.7	$2.8^{+2.9}_{-2.8}$	14700 ± 171	63 ± 11	0.9 ± 0.2
off	on	$12.6^{+8.4}_{-7.6}$	$0.037^{+0.035}_{-0.016}$	7.8 ± 0.8	$3.1^{+3.0}_{-2.8}$	14695 ± 171	63 ± 11	0.9 ± 0.2
off	off	0	0	7.5 ± 0.7	2.7 ± 3.0	14702 ± 171	64 ± 11	0.9 ± 0.2
off	on	0	0	7.5 ± 0.7	2.8 ± 3.1	14706 ± 172	64 ± 11	0.9 ± 0.2
off	off	$6.4^{+7.9}_{-8.1}$	0	7.5 ± 0.7	$2.4^{+2.9}_{-2.7}$	14698 ± 171	63 ± 11	0.9 ± 0.2
off	on	$5.3^{+8.8}_{-7.7}$	0	$7.3^{+0.7}_{-0.6}$	$3.0^{+3.4}_{-3.1}$	14698 ± 171	64 ± 11	0.9 ± 0.2
8.1 ± 0.5	off	0	$0.023^{+0.029}_{-0.017}$	7.9 ± 0.4	$2.5^{+2.8}_{-2.6}$	14693 ± 171	64 ± 11	0.9 ± 0.2
8.1 ± 0.5	on	0	$0.041^{+0.033}_{-0.027}$	8.0 ± 0.5	$3.2^{+3.0}_{-2.9}$	14703 ± 171	64 ± 11	0.9 ± 0.2
8.1 ± 0.5	off	$-0.1^{+9.2}_{-6.6}$	$0.022^{+0.033}_{-0.016}$	$7.9^{+0.4}_{-0.5}$	$2.7^{+2.9}_{-2.7}$	14698 ± 171	63 ± 11	0.9 ± 0.2
8.1 ± 0.5	on	$3.4^{+5.7}_{-4.6}$	$0.038^{+0.023}_{-0.018}$	8.0 ± 0.4	3.0 ± 2.7	14702 ± 171	64 ± 11	0.9 ± 0.2
8.1 ± 0.5	off	0	0	7.9 ± 0.4	$2.8^{+2.7}_{-2.9}$	14697 ± 171	64 ± 11	0.9 ± 0.2
8.1 ± 0.5	on	0	0	7.8 ± 0.4	$3.0^{+3.0}_{-2.9}$	14701 ± 171	65 ± 11	0.9 ± 0.2
8.1 ± 0.5	off	$6.1^{+10.3}_{-8.6}$	0	7.8 ± 0.4	$2.7^{+2.7}_{-2.9}$	14701 ± 171	64 ± 11	0.9 ± 0.2
8.1 ± 0.5	on	$5.4^{+7.7}_{-8.5}$	0	7.9 ± 0.4	$3.0^{+3.0}_{-2.9}$	14705 ± 171	65 ± 11	0.9 ± 0.2

when the requirement for the star to be on the MS is enforced. Owing to the much more favourable S statistic, and the influence on the stellar parameters, we elect to use results which account for the MS relationship. Adding a linear velocity trend gave no discernible difference in the quality of the fit to the spectroscopic data, and with a magnitude of $|\dot{\gamma}| < 13\,\mathrm{m\,s}^{-1}\,\mathrm{yr}^{-1}$ we conclude that no such trend is present in the system. Adding a prior on the spectroscopic $v \sin I$ made little difference to the results despite the relatively rapid rotation, so we again choose the simpler route and neglect such a prior. Finally, we choose a circular solution; the F-test of Lucy & Sweeney (1971) shows that the small eccentricity values returned when e is allowed to float are insignificant.

Our optimal solution is therefore that obtained with no $v \sin I$ prior, no velocity trend, the MS prior active, and $e = 0$. This set of priors gives $\lambda = 2.8^\circ \pm 3.1$, leading to the conclusion that the WASP-31 system is well-aligned. It is worth noting that this would be the conclusion whichever combination of priors we chose, as all of the values of λ that we obtained lie within 1.2σ of 0^o. The impact parameter is $0.77^{+0.01}_{-0.02}$. The stellar rotation for this solution has a value of $v \sin I = 7.5 \pm 0.7\,\mathrm{km\,s}^{-1}$. As with our result for WASP-16 this is slower than the spectroscopic value, but in this case the value agrees to within 1σ. Again, an alternative analysis using the calibration of Gray (1992) returns a value of $v \sin I$ ($7.5 \pm 0.5\,\mathrm{km\,s}^{-1}$) more similar to our MCMC result. WASP-31 is not included in the sample of Schlaufman (2010) owing to its time of publication. In order to check the possibility of misalignment along the line-of-sight, we follow the method of Schlaufman and calculate the rotation statistic, Θ. The age of WASP-31 A is somewhat uncertain however; its lithium abundance, gyrochronology and the presence of a close companion all suggest ages of ≈ 1 Gyr, whilst previous stellar model fits imply an older age of 4 ± 1 Gyr. We reassess the isochronal fit for the system, obtaining ages of $4.0^{+1.8}_{-1.0}$ Gyr (Padova models), $2.8^{+1.4}_{-1.0}$ Gyr (Yonsei-Yale models), $3.5^{+2.3}_{-1.3}$ Gyr (Teramo models) and $2.8^{+1.6}_{-1.2}$ Gyr (VRSS models). Using these estimates we calculate values of $\Theta = -4.5$, -3.0, -3.7 and -2.8 respectively; WASP-31 is therefore rotating more rapidly than expected given its age in both cases. The chance of significant misalignment along the line-of-sight therefore seems slim; the inclination of the WASP-31 b's orbit is $84.6 \pm 0.2^\circ$, leaving little room for an increase in rotation velocity owing to line-of-sight misalignment.

5 INTEGRATION INTO THE ENSEMBLE OF RESULTS

The analysis of W10 provides a good starting point for integrating our new results into the existing ensemble of RM measurements. Fig. 7 reproduces fig. 2 from their paper, with the addition of all complete RM measurements made since its publication (except WASP-23 (Triaud et al. 2011), for which the result is still highly uncertain, and WASP-26 (Anderson et al. 2011), which showed only a very low amplitude and was classed as a non-detection); we list these planets in Table 5. We also elect to include most of the systems that W10 disregard during their analysis as having insufficiently precise measurements of λ [2] in order to provide a full picture

[2] HAT-P-2, CoRoT-1, CoRoT-3, HD149026, Kepler-8, TrES-1 and TrES-2. See references within W10. Although WASP-2 has a measured value for λ, the most recent analysis of the system failed to detect a signal (Albrecht et al. 2011) and thus we continue to exclude this system.

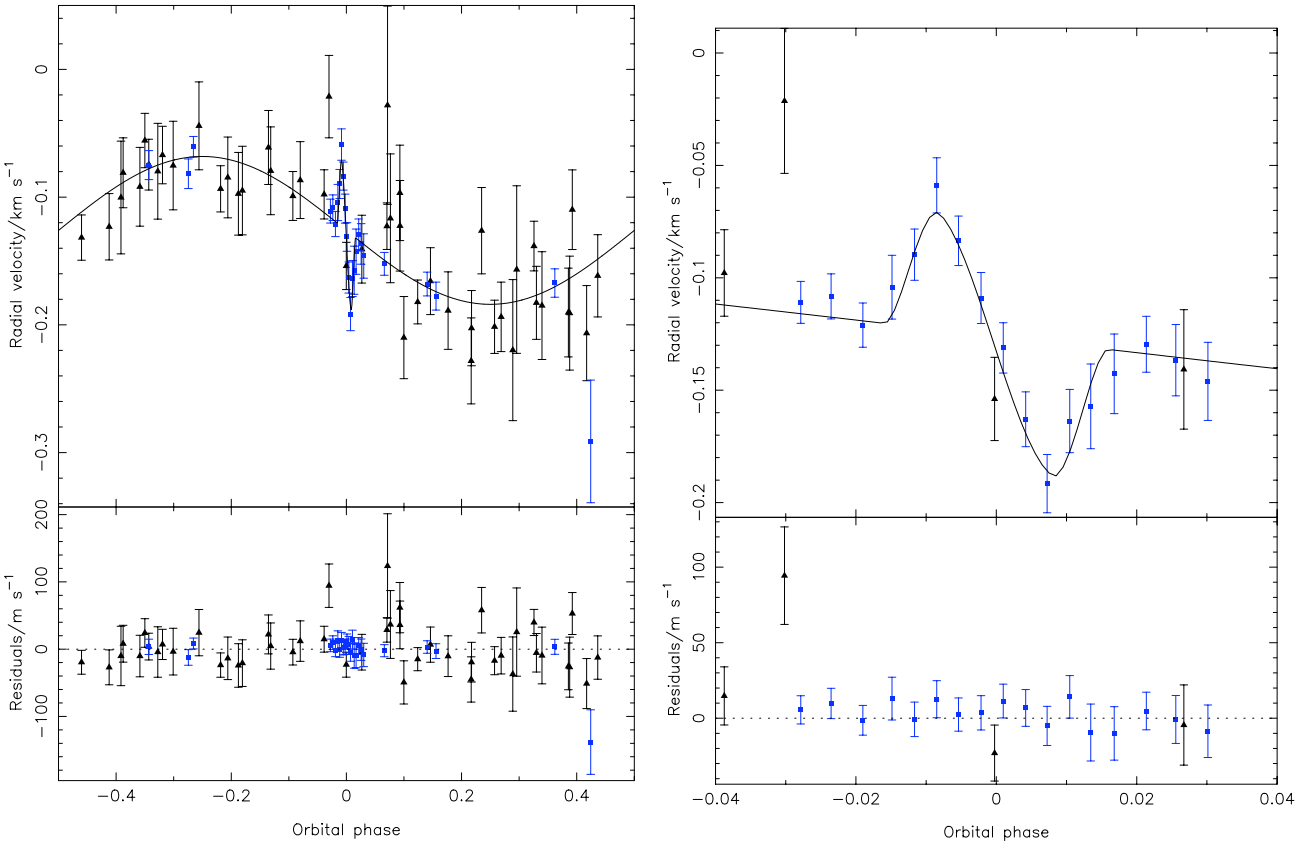

Figure 5. Results from the fit to the data for our adopted solution for WASP-31, with a circular orbit, no prior on the spectroscopic $v \sin I$, no long-term radial velocity trend, and the mass-radius relationship applied. Legend as for Fig. 1.

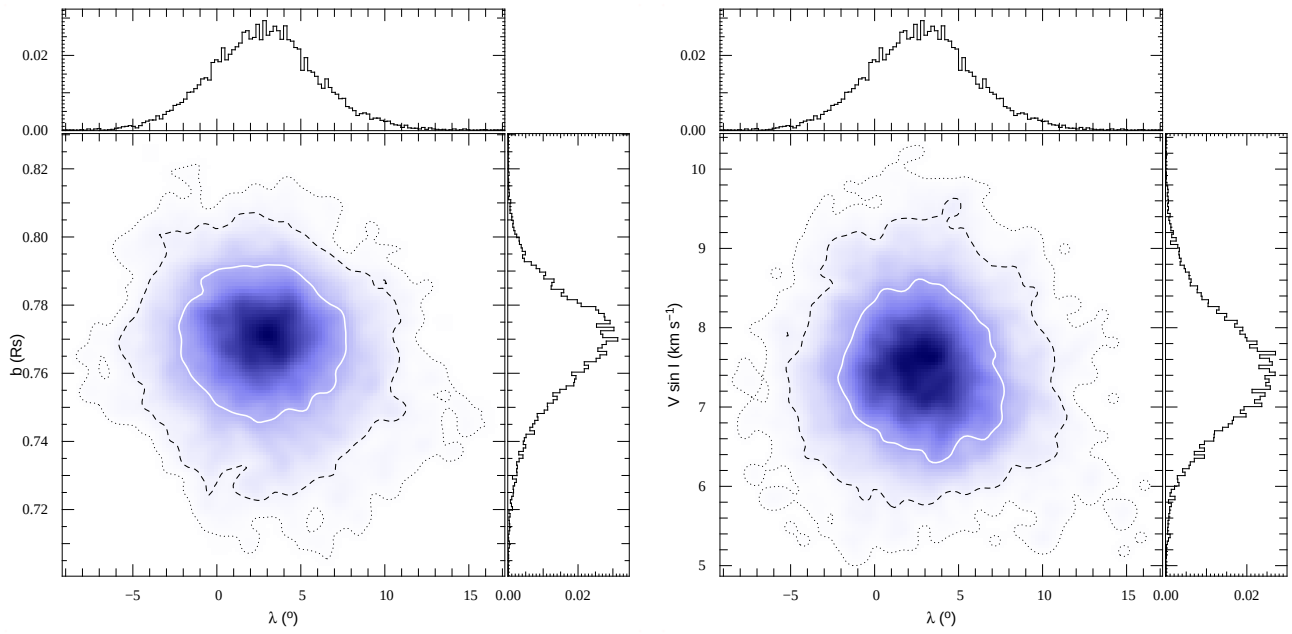

Figure 6. Posterior probability distributions, derived from the Markov chain, for the fit to the data for WASP-31 described in Fig. 5. Key as for Fig. 'reffig:W16prob. *Left:* b and λ. *Right:* $v \sin I$ and λ. $\lambda = 0$ lies well within the main body of the distribution.

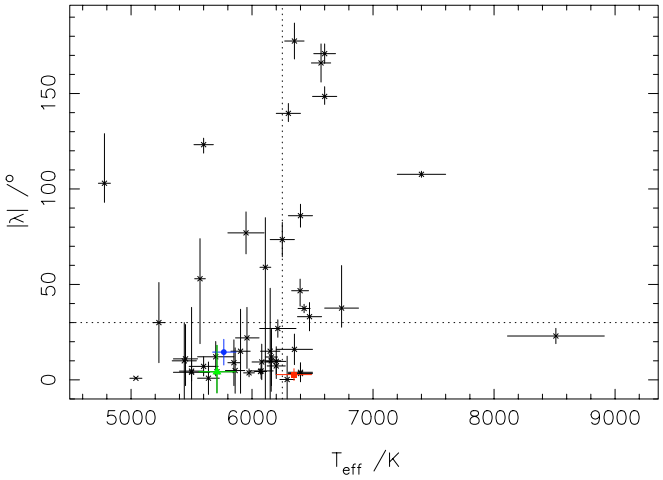

Figure 7. Projected stellar obliquity, λ, as a function of stellar effective temperature for all systems with confirmed measurements. WASP-16 is marked by a green, filled triangle, WASP-25 by a blue, filled circle, and WASP-31 by a red, filled square. The vertical dotted line marks the distinction between 'cool' and 'hot' systems, whilst the horizontal dotted line marks 30°, the angle above which a system is considered to be misaligned in W10 and T10.

of the current state of RM analysis. Whilst it is true that making a definitive statement regarding alignment is more difficult for these systems owing to their large uncertainties, the criteria for granting misaligned status should take account of this. We are also interested in comparing our new measurements to the general form of the current ensemble. Omitting the systems listed above does not simplify this task, so we elect to include them.

WASP-31 has an effective temperature of 6300 ± 100 K, which falls with 1σ of the border between the 'hot' and 'cool' categories of W10, albeit tending towards the 'hot' side. We cannot therefore draw any conclusions as to how it affects the trend proposed in that paper.

With an effective temperature of 5750 ± 100 K, WASP-25 falls into the 'cool' category (Teff $\leqslant$ 6250 K) of W10, which they find to be preferentially aligned – their sample gives a probability of misalignment for 'cool' stars of 0.17. Updating this result using our expanded sample changes the probability to 0.20 using either the criterion of W10, or to 0.13 using the criterion of $|\lambda| > 30^o$ from T10. It is worth noting here that the apparently large differences in misalignment probability between the two criteria are an artefact of the sample size, which is still relatively small at 48 systems (30 'cool', 18 'hot'). Switching between the two criteria only changes the number of aligned systems by two for the 'cool' sub-sample, and has no effect on the number of misaligned systems in the 'hot' sub-sample. Under both criteria the apparent alignment of WASP-25 b's orbit is in accordance with the W10 hypothesis. WASP-16, $T_{eff} = 5700 \pm 150$ is also classified as a 'cool' system. All available information points towards this system being well-aligned, and it therefore fits well with the hypothesis of W10.

The final interesting point about Fig. 7 is the apparent lack of systems with mildly retrograde, close to polar orbits. There are currently only two systems with $80^o \leqslant \lambda \leqslant 110^0$, and only one more with $110° \leqslant \lambda \leqslant 140°$ This relatively unpopulated region is less noticeable when considering ψ owing to the increased size of the error bars, but it is still apparent. We speculate that truly polar orbits are perhaps unstable for some reason. Or perhaps it is simply our inability to determine the inclination of the stellar rotation axis that is at fault. It may be that some 'aligned' systems actually have close to polar orbits if this angle is accounted for. It may also be that we simply have yet to observe very many systems in this region of the parameter space, and future publications may provide the data to fill this underpopulated area.

It has not been remarked upon before in this context, but a drop in the number of systems at mid-range obliquity angles is clearly predicted by the theoretical ψ angular distribution of Fabrycky & Tremaine (2007). It also clearly shows up in the angular distribution for the complete set of known obliquity angles, fig. 10 in T10. We reproduce this figure in Fig. 8, adding the probability distributions of the planets in Table 5 as well as those of the planetary systems from this study. ψ, the true misalignment angle, is given by

$$\cos\psi = \cos I \cos i + \sin I \sin i \cos\lambda, \quad (2)$$

where I is the inclination of the stellar rotation axis to the line-of-sight, and i is the inclination of the orbital axis to the line-of-sight. To calculate the ψ distribution for each planet we carried out 10^6 Monte Carlo simulations, drawing values for I from a uniform $\cos I$ distribution to represent the case in which stellar rotation axes are randomly oriented on the sky. We also accounted for the error bars on i and λ by drawing values from a Gaussian distribution with our optimal solution values as the mean values, and scaled to the uncertainties in those values. The individual planets' distributions were then summed to produce our total distribution, which is similar to that of T10, and still compares favourably to the theoretical histogram from Fabrycky & Tremaine (2007). The drop in probability at mid-range angles is in line with the underpopulated region of Fig. 7, and our additions bring the primary, low-angle peak closer in shape to the theoretical distribution. The overall shape of the secondary peak is less clear; it is still dominated by contributions from individual systems owing to the smaller number of planets with strongly misaligned orbits as compared to the number of aligned or weakly misaligned systems, but appears as though it may be broader and more shallow than the theoretical prediction.

Fig. 8 requires the assumption that the I, the stellar inclination, is isotropic and that the angular distribution is unimodal. However the discussion of W10 implies that the distribution is in fact bimodal. A clearer demonstration of the agreement between theoretical predictions and current observations is therefore to look at the distribution in λ. This requires the converse transformation of the predicted ψ distribution of Fabrycky & Tremaine (2007) into λ.

We reproduce the lower panel of fig. 9 from T10, taking into account the additional measurements of λ from Table 5. For HAT-P-7 and HAT-P-14, both of which have published $\lambda > 180.0°$, we used the negative angle equivalent $(360 - \lambda)$. This cumulative λ distribution avoids both of the assumptions inherent in Fig. 8. Agreement between the observational data and the theoretical predictions of Fabrycky & Tremaine (2007) has been improved, particularly for low- to mid-range angles, but the observational data are still slightly lacking in high obliquity systems compared to the theoret-

Table 5. Relevant data for the planetary systems for which the Rossiter-McLaughlin effect has been characterised since the publication of W10. We add these systems to the Winn et al. sample to bring the ensemble of results up to date and allow us to better analyse the place of WASP-25 and WASP-31 within that ensemble.

System	$i/^\circ$	$v \sin I / \mathrm{km\,s^{-1}}$	$T\mathrm{eff}/\mathrm{K}$	$\lambda/^\circ$	Reference
CoRoT-18	$86.5^{+1.4}_{-0.9}$	8.0 ± 1.0	5440 ± 100	10 ± 20	Hébrard et al. (2011)
HAT-P-4	$88.76^{+0.89}_{-1.38}$	5.83 ± 0.35	5860 ± 80	4.9 ± 11.9	Winn et al. (2011)
HAT-P-6	85.51 ± 0.35	7.5 ± 1.6	6570 ± 80	166 ± 10	Hébrard et al. (2011)
HAT-P-8	87.5 ± 1.4	14.5 ± 0.8	6200 ± 80	$-17^{+9.2}_{-11.5}$	Latham et al. (2009); Moutou et al., (2011)
HAT-P-9	86.5 ± 0.2	12.5 ± 1.8	6350 ± 150	-16 ± 8	Shporer et al. (2009); Moutou et al., (2011)
HAT-P-11	$89.17^{+0.46}_{-0.60}$	$1.00^{+0.95}_{-0.56}$	4780 ± 50	103^{+26}_{-10}	Winn et al. (2010)
HAT-P-14	83.52 ± 0.22	8.18 ± 0.49	6600 ± 90	189.1 ± 5.1	Winn et al. (2011)
HAT-P-16	86.6 ± 0.7	3.9 ± 0.8	6158 ± 80	-10.0 ± 16	Buchhave et al. (2010); Moutou et al., (2011)
HAT-P-23	85.1 ± 1.5	7.8 ± 1.6	5905 ± 80	15 ± 22	Bakos et al. (2011); Moutou et al., (2011)
HAT-P-30	83.6 ± 0.4	3.07 ± 0.24	6304 ± 88	73.5 ± 9.0	Johnson et al. (2011)
KOI-13.01	85.0 ± 0.4	65 ± 10	8511 ± 400	23 ± 4	Barnes, Linscott & Shporer (2011)
WASP-1	90 ± 2	$0.7^{+1.4}_{-0.5}$	6110 ± 45	-59^{+99}_{-26}	Albrecht et al. (2011)
WASP-7	$87.2^{+0.9}_{-1.2}$	14 ± 2	6400 ± 100	86 ± 6	Southworth et al. (2011); Albrecht et al. (2012)
WASP-19	$79,4 \pm 0.4$	4.63 ± 0.26	5500 ± 100	4.6 ± 5.2	Hellier et al. (2011)
WASP-22	88.26 ± 0.91	4.42 ± 0.34	5958 ± 98	22 ± 16	Anderson et al. (2011)
WASP-24	83.64 ± 0.29	7.0 ± 0.9	6075 ± 100	-4.7 ± 4.0	Simpson et al. (2010)
WASP-38	$88.83^{+0.51}_{-0.55}$	8.58 ± 0.39	6150 ± 80	15^{+33}_{43}	Simpson et al. (2010)
XO-3	82.5 ± 1.5	18.4 ± 0.2	6430 ± 50	37.4 ± 2.2	Winn et al. (2009); Hirano et al. (2011)
XO-4	88.8 ± 0.6	8.9 ± 0.5	6397 ± 70	-46.7 ± 7.1	Narita et al. (2010)

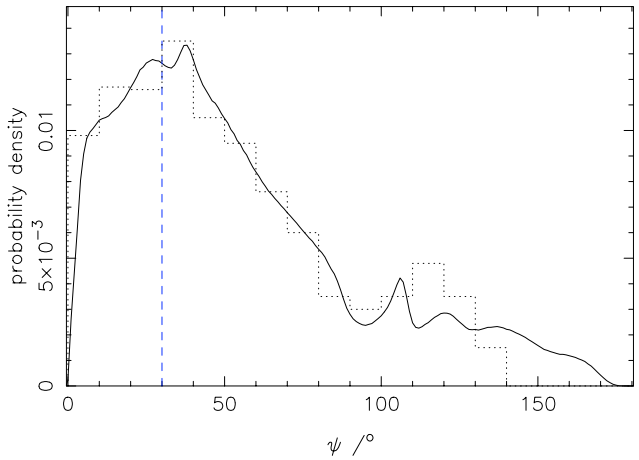

Figure 8. The total distribution of the true obliquity angle, ψ, for the complete sample of systems for which λ has been measured. The dotted histogram represents the theoretical distribution of Fabrycky & Tremaine (2007). The dashed line represents the limit of $\psi = 30°$ above which a system is considered to be misaligned. The overall forms are comparable, and the total ψ distribution is similar to fig. 10 of T10. The shape of the primary peak agrees well with theoretical predictions. The overall shape of the secondary, high angle peak in the distribution is less clear, but may be more shallow and broader than anticipated. The sudden drop in probability density at mid-range angles, around $\psi \approx 90^o$, has become more pronounced when compared to the distribution of T10.

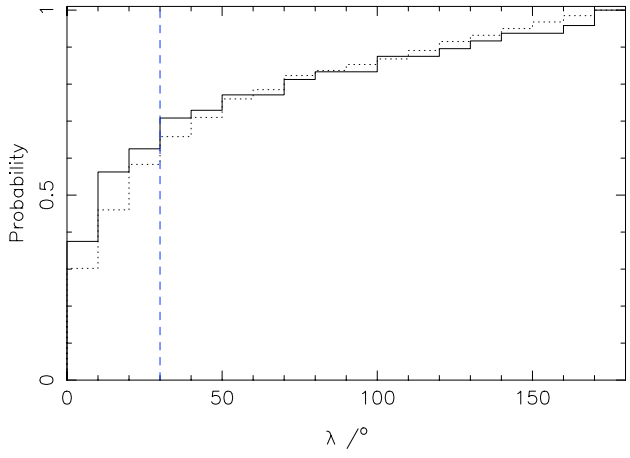

Figure 9. Cumulative probability histogram for λ. The solid line denotes observational data, whilst the dotted line denotes the theoretical distribution of Fabrycky & Tremaine (2007), converted from ψ to λ. The vertical blue, dashed line marks $\lambda = 30°$, the limit above which a planetary orbit is considered to be misaligned. The agreement between the two distributions has improved with the addition of measurements made since the publication of T10, particularly at mid-range angle, prograde orbits, but the observational data is still lacking in high obliquity systems compared to the theoretical prediction.

ical histogram, whilst showing more low-obliquity systems than expected.

6 A NEW MISALIGNMENT TEST

The Rossiter-McLaughlin effect has now been measured for 48 transiting exoplanets, but as of yet there seems little consensus as to the best way of classifying them as aligned or misaligned. For most of the systems with measurements of λ this is not a serious problem; either $|\lambda| > 90^o$, or the error bars are such that the obliquity is consistent with zero. But as the number of RM measurements continues to grow, there will be an increasing number of systems in a similar situation to WASP-25, which exhibits a mildly asymmetrical RM anomaly but does not fulfil any of the current misalignment criteria.

There are two main criteria currently in use by the community. W10 use $|\lambda| > 0^o$ at $\geqslant 3\sigma$ significance to define a misaligned system. T10 take $|\lambda| > 30^o$ as their threshold, on the basis that errors in the obliquity angle are of the order of 10^o, and therefore this gives 3σ significance as well. We would like to introduce a new test for misalignment that takes a completely different approach to these.

We consider the set of WASP planets for which the RM effect has been characterised using RV data, including the systems presented in this study. We neglect the WASP-33 system for which the misalignment angle has been measured only through Doppler tomography (Collier Cameron et al. 2010), and disregard the ambiguous results for WASP-23 (Triaud et al. 2011) and WASP-2 (Albrecht et al. 2011). For reasons of consistency we use the RV based solution of Tripathi et al. (2010) for our intial conditions for WASP-3, rather than the more recent tomographical study of Miller et al. (2010). The full set of planets sample is listed in Table 6.

Our test is based on the Bayesian Information Criterion (BIC) (Liddle 2007),

$$\mathrm{BIC} = \chi^2_{RV} + k\ln(n), \tag{3}$$

where k is the number of parameters and n is the number of data. Changing the value of λ only affects the form of the model RV curve in-transit; we therefore just consider those RV points that lie within a region of the RV curve around phase 0 defined by the fractional transit width when computing the second term of the BIC. The number of parameters changes according to the choice of priors applied to the MCMC run; adding a long-term RV trend, fitting the RM effect, and allowing the eccentricity to float all add one or more additional parameters to the model.

We carry out two MCMC analyses for each of the systems in our sample, using the same combination of priors for both. The first analysis allows both $\sqrt{v\sin I}\cos\lambda$ and $\sqrt{v\sin I}\sin\lambda$ to float, whilst the second forces an aligned orbit by fixing $\sqrt{v\sin I}\sin\lambda = 0$. We calculate the BIC for both runs, before calculating $B = \mathrm{BIC}_{\mathrm{align}}/\mathrm{BIC}$. For the 3 systems presented herein we use our adopted solutions, and carry out an additional run to provide the aligned case. We plot the results for all of the systems as a function of the sky-projected alignment angle.

We find several distinct groups of systems within our results, which lead us to define three categories of alignment into which systems with RM measurements can be classified. Five systems, including WASP-16 and WASP-31, were found to have$B \leqslant 0.980$, implying that the model with $\lambda = 0$ provides a better fit that the free-floating λ model. Of these five systems, all would be classified as aligned according to either of the existing misalignment criteria. A further four systems, including WASP-25, are clustered around $B = 1.00$, forming a distinct group in figure 10b. Forcing an aligned orbit would seem to make little difference to the quality of the fit between data and model in these cases. Of these systems three would clearly be classed as aligned according to W10 and T10, but the fourth (WASP-1) would actually be classed as misaligned according to W10. The remaining systems clearly lie distinct from those discussed so far, and many are clearly classifiable as misaligned, with $|\lambda| > 100^\circ$ and $B > 1.5$.

In light of these results, we define three categories of alignment. Systems for which $B \leqslant 0.99$ we classify as misaligned. Those with $B \geqslant 1.01$ we classify as aligned. Systems falling between these categories, with $0.99 < B < 1.01$ we classify as of indeterminate alignment. We would also define a fourth category, that of 'no detection', as containing those systems with $v\sin I$ consistent with 0 to within 1σ, but our current sample contains no systems that meet this requirement.

Some of the systems in Table 6 warrant a little more examination. WASP-16, despite the relatively poor quality of the RM data that we obtained, can be more strongly considered aligned than WASP-31 with its high quality data. This is an interesting, if puzzling result, but does provide further evidence to support our previous conclusion of an aligned system for WASP-16. WASP-25 is classified as undetermined under our new criteria, possibly owing to the relatively poor match between the shape of the RM anomaly and the best-fitting model. However we note that it lies very close to the boundary between the 'undetermined' and 'misaligned' categories. Our new MCMC runs for WASP-1 and WASP-4 produce very large error bars on λ, but end up in different categories despite both failing the T10 criterion of misalignment. Examining their respective RM anomalies we note that both have very low amplitudes, but that the data for WASP-4 is of significantly better quality than that for WASP-1. It is likely that this is responsible for the difference in classification. In addition, T10 noted a substantial correlation between λ and $v\sin I$ for WASP-4, arising due to the low impact parameter, which may be producing the large lower error. WASP-38 also exhibits a significant error bar on λ, and we again note that the RM data is again of somewhat poor quality. New observations of WASP-38 using HARPS may help to improve the quality of the results for the system, allowing us to draw firmer conclusions (Brown et al, *in prep.*).

7 CONCLUSIONS

We have presented analysis of the Rossiter-McLaughlin effect for WASP-16, WASP-25 and WASP-31. We find WASP-16 to have a very low amplitude signal, but the use of two complete spectroscopic transits has enabled us to determine a sky-projected alignment angle of $\lambda = -4.2^{\circ}{}^{+11.0}_{-13.9}$. For WASP-25 we find a mildly asymmetric RM anomaly with $\lambda = 14.6^\circ \pm 6.7$, and for WASP-31 we obtain $\lambda = 2.8^\circ \pm 3.1$, indicating a well-aligned system.

Since WASP-31 lies so close to the effective temperature that divides the classes of 'hot' and 'cool' planet hosts, we cannot say how its alignment affects the pattern proposed

Table 6. Relevant data for our new misalignment criterion, for a sample of WASP planets with existing Rossiter-McLaughlin measurements. λ values are those obtained from our new MCMC analyses. BIC values were calculated from the spectroscopic χ^2 values, using the number of in-transit RV measurements only. Our new misalignment criterion defines systems with a BIC ratio $B \geqslant 1.01$ as misaligned, those with $B \leqslant 0.99$ as aligned, and those with $0.99 < B < 1.01$ as of indeterminate status.

System	reference	$\lambda/^\circ$	$v \sin I/\mathrm{km\,s^{-1}}$	BIC	$\mathrm{BIC_{align}}$	ΔBIC	B
WASP-1	Albrecht et al. (2011)	$60.2^{+23.3}_{-126.6}$	1.3 ± 0.5	255.2 ± 22.6	256.7 ± 22.7	1.5	1.006
WASP-3	Tripathi et al. (2010)	$37.9^{+9.3}_{-11.8}$	$12.9^{+1.1}_{-0.8}$	294.7 ± 24.3	308.0 ± 24.8	13.3	1.045
WASP-4	Triaud et al. (2010)	$42.0^{+14.3}_{-75.6}$	$2.5^{+0.4}_{-0.3}$	86.8 ± 13.2	91.3 ± 13.5	4.5	1.052
WASP-5	Triaud et al. (2010)	$26.2^{+8.1}_{-6.8}$	3.5 ± 0.2	186.0 ± 19.3	199.2 ± 20.0	12.1	1.071
WASP-6	Gillon et al. (2009)	$-7.5^{+20.9}_{-19.1}$	$1.7^{+0.3}_{-0.2}$	134.7 ± 16.4	132.0 ± 16.2	-2.7	0.980
WASP-7	Albrecht et al. (2012)	$85.0^{+9.4}_{-8.0}$	$26.3^{+1.3}_{-1.2}$	285.8 ± 23.9	451.7 ± 30.1	165.9	1.580
WASP-8	Queloz et al. (2010)	$-106.7^{+3.0}_{-3.5}$	$2.8^{+0.4}_{-0.3}$	380.3 ± 27.8	1092.5 ± 46.7	712.2	2.873
WASP-14	Joshi et al. (2009)	$-28.0^{+5.0}_{-5.5}$	2.8 ± 0.3	171.2 ± 18.5	193.5 ± 19.7	22.3	1.130
WASP-15	Triaud et al. (2010)	$-133.8^{+11.7}_{-9.5}$	$4.5^{+0.4}_{-0.3}$	154.4 ± 17.6	555.7 ± 33.3	401.3	3.599
WASP-17	Triaud et al. (2010)	$-134.5^{+5.3}_{-7.1}$	9.8 ± 0.3	342.7 ± 26.2	986.9 ± 44.4	644.2	2.880
WASP-18	Triaud et al. (2010)	$20.5^{+10.5}_{-11.5}$	12.9 ± 0.3	118.8 ± 15.4	119.0 ± 15.4	0.2	1.002
WASP-19	Hellier et al. (2011)	$-1.6^{+5.6}_{-5.4}$	3.2 ± 0.2	81.5 ± 12.8	79.8 ± 12.6	-1.7	0.979
WASP-24	Simpson et al. (2010)	$-6.9^{+5.4}_{-5.8}$	$5.1^{+0.4}_{-0.3}$	123.1 ± 15.7	119.8 ± 15.5	-3.3	0.973
WASP-38	Simpson et al. (2010)	$-6.1^{+3.3}_{-38.7}$	8.2 ± 0.3	241.3 ± 22.0	240.8 ± 21.9	-0.5	0.998
WASP-16	this study	$-4.2^{+11.0}_{-13.9}$	$1.2^{+0.4}_{-0.5}$	115.6 ± 15.2	112.1 ± 15.0	-3.5	0.970
WASP-25	this study	14.6 ± 6.7	2.9 ± 0.3	116.5 ± 15.3	117.5 ± 15.3	0.8	1.009
WASP-31	this study	2.8 ± 3.1	7.5 ± 0.7	73.7 ± 12.1	72.2 ± 12.0	-1.5	0.980

by W10. WASP-25 on the other hand at first appears to strengthen their hypothesis, with the existing misalignment criteria of both W10 and T10 labelling it aligned. We have also presented a new method for determining the alignment or otherwise of an exoplanetary orbit. Our test is based on the BIC statistic, and bases the misalignment or alignment of a system on the ratio of the values of the BIC for the free λ case and the aligned case. We classify systems with $B \geqslant 1.01$ as misaligned, those with $B \leqslant 0.99$ as aligned, and those with $0.99 \leqslant B \leqslant 1.01$ as of indeterminate classification. WASP-25 falls in this last category, albeit very close to the boundary with the 'misaligned' classification.

The results presented herein bring the analysis of the ensemble of systems with confirmed stellar obliquities up to date. Our results have done little to change the overall picture presented by T10, instead strengthening the agreement with theoretical predictions for the distributions of both the projected and true stellar obliquities. We should not be too hasty to assume that we have solved the problem of hot Jupiter migration however; new discoveries are constantly causing us to re-evaluate our current understanding.

ACKNOWLEDGMENTS

The authors would like to thank the referee, Josh Winn, for his insightful comments and constructive suggestions. D. J. A. Brown would also like to thank Teryuki Hirano for assistance with improving the RM modelling, and Simon Albrecht for helpful discussions regarding analysis of these systems. M. Gillon is FNRS Research Associate. The WASP Consortium consists of representatives from the Universities of Keele, Leicester, The Open University, Queens University Belfast and St Andrews, along with the Isaac Newton Group (La Palma) and the Instituto de Astrofisca de Canarias (Tenerife). The SuperWASP and WASP-S cameras were constructed and operated with funds made available from Consortium Universities and PPARC/STFC. This research has made use of NASA's Astrophysics Data System Bibliographic Services, and the ArXiv preprint service hosted by Cornell University.

REFERENCES

Albrecht S, Reffert S., Snellen I., Quirrenbach A., Mitchell D. S., 2007, A&A, 474, 565
Albrecht S., Reffert S., Snellen I. A. G., Winn J. N., 2009, Nature, 461, 373
Albrecht S. et al., 2011, ApJ, 738, 50
Albrecht S., Winn J. N., Butler R. P., Crane J. D., Shectman S. A., Thompson I. B., Hirano T., Wittenmyer R. A., 2012, ApJ, 744, 189
Anderson D. R. et al., 2011, A&A, 531, A60
Anderson D R et al, 2011, A&A, 534
Bakos G Á et al., 2011, ApJ, 742, 116
Baliunas S. L. et al., 1995, ApJ, 438, 269
Barnes S. A., 2007, ApJ, 669, 1167
Barnes J. W., Linscott E., Shporer A., 2011, ApJ, 197, 10
Bouchy F. et al., 2008, A&A, 482, L25
Bruntt H. et al., 2010, MNRAS, 405, 1907

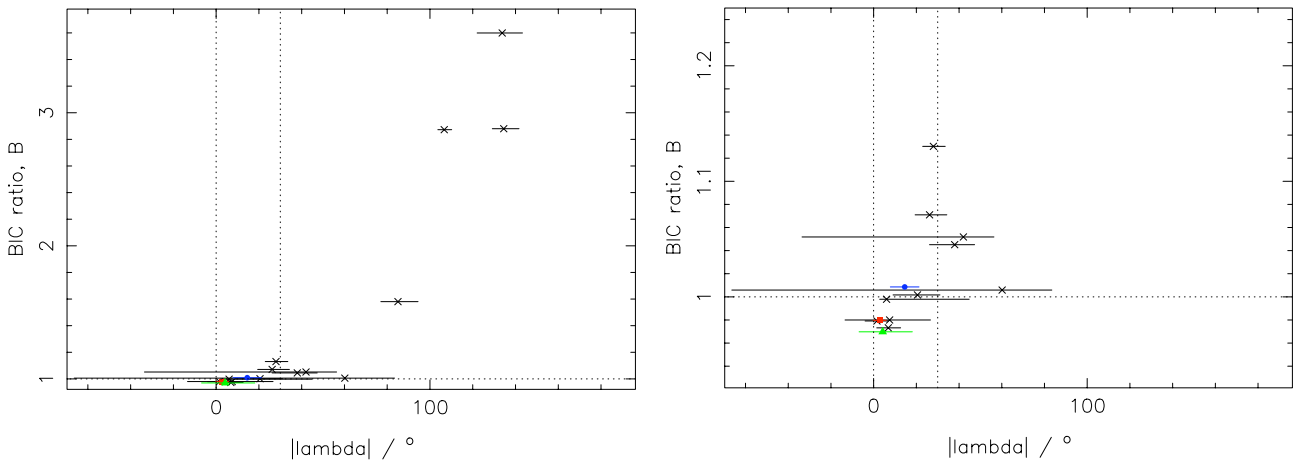

Figure 10. B as a function of λ for the sample of planets in Table 6, as well as the systems presented in this study. WASP-16 is denoted by a filled, green triangle. WASP-25 is denoted by a filled, blue circle. WASP-31 is denoted by a filled, red square. The horizontal dotted line marks $B = 1.00$. The two vertical dotted lines denote $|\lambda| = 0°$ and $|\lambda| = 30°$, the existing criterion for misalignment. *Left:* All data. *Right:* A close-up of the heavily populated region in the lower left of the plot, around $B = 1.00$ and $|\lambda| = 0°$. This shows the separation of the systems into several distinct groupings, which lead us to define three categories of alignment. This changes the existing classification of some systems.

Buchhave L. A. et al., 2010, ApJ, 720, 1118
Collier Cameron A. et al., 2007, MNRAS, 380, 1230
Collier Cameron A., Bruce V. A., Miller G. R. M., Triaud A. H. M. J., Queloz, D., 2010, MNRAS, 403, 151
Collier Cameron A. et al., 2010, MNRAS, 407, 507
Claret A., 2000, A&A, 363, 1081
Demarque P., Woo J.-H., Kim Y.-C., Yi S.K̃., 2004, ApJS, 155, 667
Enoch B., Collier Cameron A., Parley N. R., Hebb L., 2010, A&A, 516, A33
Enoch B et al., 2011, MNRAS, 410, 1631
Fabrycky D., Tremaine S., 2007, ApJ, 669, 1298
Fabrycky D. C., Winn J. N., 2009, ApJ, 696, 1230
Ford E., 2006, ApJ, 642, 505
Gillon M. et al., 2009, A&A, 501, 785
Gray D.F̃., 1992, PASP, 106, 1248
Gray D.F̃., 2008, The observation and analysis of stellar photospheres, Cambridge Univ. Press, Cambridge, UK
Hébrard G. et al., 2011, A&A, 527, L11
Hébrard G. et al., 2011, A&A, 533
Hellier C., Anderson D. R., Collier-Cameron A., Miller G. R. M., Queloz D., Smalley B., Southworth J., Triaud A. H. M. J., 2011, ApJL, 730, L31
Hirano T., Suto Y., Taruya A., Narita N., Sato B., Johnson J A., Winn J N., 2010, ApJ, 709, 458
Hirano T., Narita N., Sato B., Winn J.Ñ., Aoki W., Tamura M., Taruya A., Sato Y., 2011, PASJ, 63, L57
Hirano T., Suto Y., Winn J.Ñ., Taruya A., Narita N., Albrecht S., Sato B., 2011, ApJ, 742, 69
James D. J. et al., 2010, A&A, 515, A100
Johnson J. A., Winn, J N., Albrecht S., Howard A W., Marcy G W., Gazak J. Z, 2009, PASP, 121, 1104
Johnson J. A. et al., 2011, ApJ, 735, 24
Joshi Y. C. et al., 2009, MNRAS, 392, 1532
Knutson H. A., Charbonneau, D., Allen L E., Burrows A., Megeath S. T., 2008, ApJ, 673, 526
Kozai Y., 1962, AJ, 67, 591
Latham D. et al., 2009, ApJ, 704, 1107
Liddle A. R., 2007, MNRAS, 377, L74
Lidov M. L., 1962, PLANSS, 9, 719
Lin D. N. C., Bodenheimer P., Richardson D. C., 1996, Nature, 380, 606
Lister T. A. et al., 2009, ApJ, 703, 752
Lucy L. B., Sweeney M. A., 1971, AJ, 76, 544
Marigo P., Girardi L., Bressan A., Groenewegen M.Ã.T̃., Silva L., Granato G.L̃., 2008, A&A, 482, 883
Mayor M. et al., 2003, The Messenger, 114, 20
McLaughlin D. B., 1924, ApJ, 60, 22
Meibom S., Mathieu R. D., Stassun K. G., 2009, ApJ, 695, 679
Miller G. R. M. et al., 2010, A&A, 523, A52
Montes D., Saar S. H., Collier Cameron A., Unruh Y. C., 1999, MNRAS, 305, 45
Moutou C et al., 2011,A&A, 533, A113
Narita N., Sato B., Hirano T., Tamura M., 2009, PASJ, 61, L35
Narita N., Hirano T., Sanchis-Ojeda R., Winn J. N., Holman M. J., Sato B., Aoki W., Tamura M., 2010, PASJ, 62, L61
Pollacco D. et al., 2006, PASP, 118, 1407
Pietrinferni A., Cassisi S., Salaris M., Castelli F., 2004, ApJ, 612, 168
Pont F. et al., 2010, MNRAS, 402, L1
Queloz D., Eggenberger A., Mayor M., Perrier C., Beuzit J. L., Naef D., Sivan J. P., Udry, S., 2000, A&A, 359, L13
Queloz D., Mayor M., Naef D., Santos N., Udry S., Burnet M., Confino B., 2000, in Bergeron J., Renzini A., eds, The VLT Opening Symposium: From Extrasolar Planets to Cosmology, Springer-Verlag, Berlin, p. 548
Queloz D. et al., 2010, A&A, 517, L1
Rossiter R. A., 1924, ApJ, 60, 15
Schlaufman K. C., 2010, ApJ, 719, 602
Shporer A. et al., 2009, ApJ, 690, 1393
Simpson E. K. et al., 2011, MNRAS, 414, 3023
Southworth J. et al., A&A, 527, A8
Tegmark M. et al., 2004, Phys. Rev. D, 69, 103501
Triaud A. H. M. J. et al., 2009, A&A, 506, 377
Triaud A. et al., 2010, A&A, 524, A25
Triaud A. et al., 2011, A&A, 531, A24
Tripathi A. et al., 2010, APJ, 715, 421
VandenBerg D.Ã., Bergbusch P.Ã., Dowler P.D̃., 2006, APJS, 162, 375
Watson C. A., Littlefair S. P., Collier Cameron A., Dhillon V.

S., Simpson E. K., 2010, MNRAS, 408, 1606
Winn, J. N. et al., 2005, ApJ, 631, 1215
Winn J. N. et al. ApJ, 2009, 700, 302
Winn J. N., Johnson, J. A., Albrecht S., Howard A. W., Marcy G. W., Crossfield I. J., Holman M. J., 2009, ApJL, 703, L99
Winn J. N., Fabrycky D., Albrecht S., Johnson J. A., 2010, ApJL, 718, L145
Winn J. N. et al., 2010, ApJL, 723, L223
Winn J. N. et al., 2011, AJ, 141, 63
Wright J. T., 2005, PASP, 117, 657

This paper has been typeset from a TEX/ LATEX file prepared by the author.

Table B1. Radial velocity data for WASP-16 obtained using the CORALIE high precision échelle spectrograph.

HJD(-2450000)	Texp/s	RV/km s^{-1}	σ_{RV}/km s^{-1}
4535.864842	900	−1.99772	0.01591
4537.849158	1427	−1.96688	0.00853
4538.858364	1800	−2.00734	0.00899
4558.780835	1800	−1.83336	0.00723
4560.709473	1800	−2.00513	0.00725
4561.688137	1800	−1.82730	0.00785
4589.705102	1800	−1.84255	0.00875
4591.706755	1800	−2.03571	0.00892
4652.495906	1800	−1.82493	0.00808
4656.551645	1800	−2.02421	0.00787
4657.577293	1800	−1.96640	0.00957
4663.539741	1800	−2.02961	0.00969
4664.616769	1800	−1.78590	0.01108
4682.521501	1800	−1.98118	0.00754
4881.869213	1800	−2.02245	0.00813
4882.801025	1800	−1.83289	0.00823
4884.737094	1800	−2.04565	0.00778
4891.805707	1800	−1.90043	0.00798
4892.723980	1800	−1.83413	0.00891
4941.728231	1800	−1.88737	0.00748
4943.730102	1800	−2.04677	0.00753
4944.739293	1800	−1.91359	0.00860
4945.799895	1800	−1.85815	0.00807
4947.745317	1800	−1.93960	0.00741
4948.673112	1800	−1.82992	0.00743
4972.707323	1800	−1.93123	0.00854
4975.733486	1800	−1.93144	0.01100
4982.647535	1800	−1.83433	0.01036
4984.642389	1800	−2.04210	0.00892
4985.694776	1800	−1.81561	0.00802
5391.544362	1800	−1.80313	0.00867

APPENDIX A: ADDITIONAL RESULTS

APPENDIX B: JOURNAL OF OBSERVATIONS

Table A1. Parameters from the best-fitting, adopted models for the three WASP planetary systems studied in the main text

System	$v \sin I$ prior	MS prior	$\dot{\gamma}/\mathrm{ms}^{-1}\mathrm{yr}^{-1}$	eccentricity	jitter $/\mathrm{m\,s}^{-1}$	$v \sin I/\mathrm{km\,s}^{-1}$	$\lambda/^\circ$
WASP-16	off	off	0	0	1.0	$1.2^{+0.4}_{-0.5}$	$-4.2^{+11.0}_{-13.9}$
WASP-25	off	on	0	0	3.6	2.9 ± 0.3	14.6 ± 6.7
WASP-31	off	on	0	0	1.0	7.5 ± 0.7	2.8 ± 3.1

Table B2. Radial velocity data for WASP-16, for the first transit obtained using the HARPS high precision échelle spectrograph on the night of 2010 March 21.

HJD(-2450000)	Texp/s	RV/km s^{-1}	σ_{RV}/km s^{-1}
5275.661171	1800	−1.80610	0.00337
5275.907691	1800	−1.78144	0.00188
5276.661941	500	−1.88264	0.00533
5276.668446	500	−1.89263	0.00546
5276.674824	500	−1.88914	0.00583
5276.681375	500	−1.87845	0.00547
5276.687753	500	−1.89900	0.00557
5276.694258	500	−1.88947	0.00569
5276.700693	500	−1.89868	0.00555
5276.707094	500	−1.89750	0.00552
5276.713599	500	−1.88945	0.00586
5276.720046	500	−1.91121	0.00614
5276.726493	500	−1.89650	0.00623
5276.732929	500	−1.88385	0.00657
5276.739376	500	−1.90596	0.00640
5276.745812	500	−1.90686	0.00704
5276.752143	500	−1.90101	0.00698
5276.758579	500	−1.91736	0.00742
5276.765605	500	−1.90950	0.00627
5276.771589	500	−1.91143	0.00447
5276.778140	500	−1.91692	0.00439
5276.784344	500	−1.91573	0.00479
5276.790838	500	−1.92779	0.00526
5276.797459	500	−1.92243	0.00510
5276.803964	500	−1.90902	0.00433
5276.810411	500	−1.92567	0.00391
5276.816441	500	−1.91540	0.00416
5276.823178	500	−1.92366	0.00424
5276.829336	500	−1.92742	0.00454
5276.835887	500	−1.92693	0.00522
5276.842334	500	−1.92962	0.00572
5276.848723	500	−1.94183	0.00699
5276.855228	500	−1.94543	0.00926
5276.861907	500	−1.92508	0.00830
5277.630948	1800	−2.02847	0.00222
5277.861599	1800	−1.99854	0.00196
5278.632376	1800	−1.82733	0.00398
5278.857922	1800	−1.79546	0.00208
5279.627285	1800	−1.84379	0.00264
5279.913540	1500	−1.91554	0.00242
5280.624797	1800	−2.03079	0.00266
5280.916481	1200	−2.00824	0.00283

Table B3. Radial velocity data for WASP-16, for the second transit obtained using the HARPS high precision échelle spectrograph on the night of 2011 May 12.

HJD(-2450000)	Texp/s	RV/km s^{-1}	σ_{RV}/km s^{-1}
5685.845943	900	−2.02724	0.00305
5687.838150	900	−1.79259	0.00383
5692.662149	900	−1.99841	0.00380
5692.796210	900	−1.96847	0.00309
5693.517817	900	−1.81013	0.00298
5693.800775	900	−1.78196	0.00285
5694.581176	600	−1.88349	0.00344
5694.588340	600	−1.88597	0.00302
5694.595389	600	−1.88670	0.00310
5694.602900	600	−1.88871	0.00305
5694.610180	600	−1.89619	0.00290
5694.616904	500	−1.89308	0.00323
5694.623386	500	−1.88547	0.00323
5694.629531	500	−1.89159	0.00309
5694.635631	500	−1.89935	0.00312
5694.641904	500	−1.89371	0.00307
5694.648003	500	−1.89694	0.00318
5694.654149	500	−1.91191	0.00298
5694.660364	500	−1.91005	0.00311
5694.666406	500	−1.91009	0.00300
5694.672609	500	−1.91343	0.00311
5694.678824	500	−1.91547	0.00327
5694.684924	500	−1.91384	0.00313
5694.691070	500	−1.91484	0.00330
5694.697227	500	−1.91701	0.00308
5694.703373	500	−1.91926	0.00308
5694.709460	500	−1.91211	0.00335
5694.715664	500	−1.91534	0.00353
5694.721821	500	−1.91948	0.00349
5694.727979	500	−1.92566	0.00346
5694.734078	500	−1.92109	0.00367
5694.740351	500	−1.92435	0.00377
5694.746612	500	−1.91926	0.00364
5694.752596	500	−1.93024	0.00354
5695.501446	900	−2.03120	0.00281

Table B4. Radial velocity data for WASP-25 obtained using the CORALIE high precision échelle spectrograph.

HJD(-2450000)	$t$exp/s	RV/km s^{-1}	σ_{RV}/km s^{-1}
4829.822664	1800	−2.57717	0.01282
4896.769798	1800	−2.65105	0.01069
4940.709168	1800	−2.71589	0.01154
4941.704336	1800	−2.61855	0.01153
4942.725717	1800	−2.57632	0.01238
4943.637434	1800	−2.61828	0.01246
4944.715466	1800	−2.67966	0.01207
4945.726530	1800	−2.61467	0.01305
4946.616622	1800	−2.58169	0.01266
4947.601618	1800	−2.64133	0.01096
4947.791245	1800	−2.68927	0.01347
4948.613002	1800	−2.70418	0.01098
4949.803142	560	−2.55132	0.01819
4950.622083	1800	−2.59141	0.01348
4951.695324	1800	−2.70149	0.01218
4971.645302	1800	−2.67821	0.02101
4972.672436	1800	−2.56129	0.01319
4973.515713	1800	−2.58676	0.01269
4974.678659	1800	−2.71413	0.01359
4975.537940	1800	−2.66695	0.01384
4976.683662	1800	−2.55567	0.01304
4982.619435	1800	−2.66448	0.02096
4983.621314	1800	−2.56777	0.01486
4983.644577	1800	−2.59698	0.01450
4984.578450	1800	−2.55837	0.01474
4985.609967	1800	−2.69905	0.01189
4995.555496	1800	−2.50858	0.01396
5009.628712	1800	−2.60564	0.01823
5010.596729	1800	−2.53871	0.02313

Table B5. Radial velocity data for WASP-25 obtained using the HARPS high precision échelle spectrograph. The point denoted by * was omitted from the analysis (see text for details).

HJD(-2450000)	$t$exp/s	RV/km s^{-1}	σ_{RV}/km s^{-1}
5296.540546	1200	−2.54661	0.00329
5296.635060	1200	−2.54381	0.00398
5297.506446	1200	−2.61464	0.00509
5297.518749	400	−2.62531	0.01007
5297.523714	400	−2.63325	0.00942
5297.528714	400	−2.60898	0.01012
5297.533807	400	−2.61031	0.01041
5297.538714	400	−2.60809	0.00999
5297.543714	400	−2.59973	0.01056
5297.548668	400	−2.59327	0.01108
5297.553761	400	−2.58984	0.01028
5297.559131	400	−2.61140	0.01786
5297.563761	400	−2.60108	0.01177
5297.568668	400	−2.60927	0.01087
5297.573715	400	−2.60539	0.01075
5297.578761	400	−2.62964	0.01153
5297.583668	400	−2.62703	0.01118
5297.588669	400	−2.61584	0.01225
5297.593715	400	−2.64141	0.01190
5297.598669	400	−2.64658	0.01232
5297.603715	400	−2.65755	0.01234
5297.608715	400	−2.67520	0.01246
5297.613761	400	−2.67558	0.01254
5297.618715	400	−2.68567	0.01244
5297.623669*	400	−2.63635	0.01215
5297.628854	400	−2.67450	0.01065
5297.633761	400	−2.65389	0.00837
5297.638715	400	−2.63022	0.00840
5297.643773	400	−2.63126	0.00885
5297.648727	400	−2.61768	0.00871
5297.653727	400	−2.63157	0.00862
5297.658681	400	−2.63982	0.00841
5297.663773	400	−2.62371	0.00834
5297.668773	400	−2.63776	0.00800
5297.673727	400	−2.64716	0.00811
5297.678727	400	−2.63753	0.00780
5297.683681	400	−2.63915	0.00781
5297.688820	400	−2.63818	0.00823
5297.693727	400	−2.64295	0.00763
5297.698774	400	−2.62870	0.00772
5297.703635	400	−2.63667	0.00757
5297.708727	400	−2.63667	0.00781
5297.713727	400	−2.63031	0.00803
5297.718681	400	−2.65168	0.00756
5297.723774	400	−2.64533	0.00785
5297.833578	1200	−2.65676	0.00352
5298.535157	1200	−2.69608	0.00406
5298.716015	1200	−2.69119	0.00285
5298.830796	1200	−2.69107	0.00287
5299.544943	1200	−2.60603	0.00327
5299.701761	1200	−2.62922	0.01842
5299.838220	1384	−2.57573	0.01224

Table B6. Radial velocity data for WASP-31 obtained using the CORALIE high precision échelle spectrograph.

HJD(-2450000)	$t$exp/s	RV/km s^{-1}	σ_{RV}/km s^{-1}
4835.809755	1800	−0.20260	0.02945
4837.773728	1800	−0.08457	0.03163
4840.765776	1800	−0.07974	0.03752
4880.767231	1800	−0.20651	0.03722
4939.627676	1800	−0.07528	0.03471
4941.567460	1800	−0.19372	0.02721
4942.654757	1800	−0.12324	0.02598
4943.610624	1800	−0.07939	0.03435
4944.555415	1800	−0.16578	0.02620
4945.544750	1800	−0.16158	0.03220
4946.591778	1800	−0.04422	0.03441
4947.555094	1800	−0.14075	0.02656
4948.588069	1800	−0.18274	0.02861
4950.597039	1800	−0.08667	0.03009
4951.608264	1800	−0.22821	0.03366
4971.548671	1800	−0.02806	0.07763
4973.489951	1800	−0.09189	0.03084
4974.608541	1800	−0.02130	0.03225
4975.511060	1800	−0.12628	0.03381
4983.595539	1800	−0.10028	0.04415
4984.467744	1800	−0.06112	0.02895
4985.530406	1800	−0.18886	0.03032
4994.508045	1800	−0.09735	0.03237
4994.531307	1800	−0.09484	0.03469
4995.463376	1800	−0.12246	0.03547
4995.486741	1800	−0.20999	0.03214
4996.459605	1800	−0.19034	0.03472
4996.482971	1800	−0.10984	0.03117
4999.536757	1800	−0.21980	0.05522
4999.560099	1800	−0.15670	0.06560
5006.521354	1800	−0.18493	0.04217
5012.492297	1800	−0.09667	0.03739
5013.497045	1800	−0.19082	0.04459
5029.465780	1800	−0.11660	0.05041
5168.846768	1800	−0.15389	0.01852
5203.782854	2700	−0.20152	0.02084
5290.715577	2700	−0.09351	0.01809
5291.699859	2700	−0.12273	0.01821
5293.696819	2700	−0.07455	0.01987
5294.733907	2700	−0.09785	0.01925
5296.704921	2700	−0.13168	0.01772
5298.693406	2700	−0.18210	0.01718
5300.589643	2700	−0.06706	0.02250
5326.628560	2700	−0.13831	0.01945
5327.604475	2700	−0.08093	0.02737
5328.608442	2700	−0.09912	0.01913
5334.544675	2700	−0.05571	0.02129

Table B7. Radial velocity data for WASP-31 obtained using the HARPS high precision échelle spectrograph.

HJD(-2450000)	$t$exp/s	RV/km s^{-1}	σ_{RV}/km s^{-1}
5298.496133	1200	−0.15638	0.00896
5298.749145	1200	−0.17218	0.00931
5299.504441	1200	−0.17141	0.01114
5299.716991	1200	−0.29541	0.04800
5300.509357	1200	−0.07910	0.01138
5300.742948	1200	−0.08587	0.01161
5301.582822	1200	−0.11516	0.00934
5301.597544	1200	−0.11250	0.01003
5301.612960	1200	−0.12527	0.00984
5301.627126	900	−0.10841	0.01418
5301.638028	900	−0.09394	0.01141
5301.648803	900	−0.06309	0.01227
5301.659393	900	−0.08776	0.01100
5301.670307	900	−0.11321	0.01136
5301.681082	900	−0.13542	0.01119
5301.691973	900	−0.16717	0.01218
5301.702354	900	−0.19579	0.01297
5301.713349	900	−0.16796	0.01407
5301.723522	900	−0.16142	0.01884
5301.734934	900	−0.14695	0.01771
5301.750477	1200	−0.13378	0.01244
5301.764794	1200	−0.14088	0.01586
5301.780360	1200	−0.15031	0.01738
5305.613529	1200	−0.18166	0.01096
5307.584640	1200	−0.06475	0.00809